Running head: Adaptive homeostasis in Arabidopsis drought response

Genetic variation associated with plastic and homeostatic growth responses to drought in Arabidopsis

Ángel Ferrero-Serrano[1] & Sarah M. Assmann[1]

[1]Biology Department, Penn State University, 208 Mueller Laboratory, University Park, PA, 16802, USA

One-sentence summary: Information on phenotype, genotype, and transcript abundance is integrated to identify both plasticity and homeostasis genes and processes associated with local adaptation to drought stress in Arabidopsis accessions of the Iberian Peninsula.

Total word count (excluding summary, references and legends):	**6,479**	Number of figures	5
		SI Figure files	1
Introduction:	521	SI Table files	1
Materials & Methods:	1,804	SI Documents	1
Results:	1,458		
Discussion:	2,696		

Summary

- Natural genetic variation influences plant responses to environmental stressors. However, the extent to which such variation underlies plastic versus homeostatic response phenotypes has been little studied.
- We quantified the extent of drought-induced changes in leaf area in a set of Iberian Arabidopsis accessions and then performed association studies correlating variation in this phenotype with genomic and transcriptomic variation.
- Drought-induced plastic reductions in relative leaf area typified accessions originating from productive environments. In contrast, homeostasis in relative leaf area typified accessions originating from unproductive environments. Genome-Wide Association Studies (GWAS), Transcriptome Wide Association Studies (TWAS), and expression GWAS (eGWAS) highlighted the importance of auxin-related processes and, in particular, the potential role of the *SMALL AUXIN UP RNA 26* (*SAUR26*) gene in conferring leaf area plasticity. Homeostatic responses in relative leaf area were associated with a diverse gene set and positively associated with a higher intrinsic water use efficiency (WUE_i) as confirmed in a TWAS metanalysis of previously published $\delta^{13}C$ measurements.
- We have identified not only candidate "plasticity genes" but also candidate "homeostasis genes" controlling leaf area. Our results demonstrate the value of a combined GWAS, TWAS, and eGWAS approach to identify mechanisms underlying phenotypic responses to stress.

Keywords: *Arabidopsis thaliana* (Arabidopsis), drought, eGWAS, GWAS, plasticity, transcriptome, TWAS, WUE_i.

INTRODUCTION

Earth is undergoing a climate change scenario resulting in extreme weather events that are increasingly frequent and variable (Easterling *et al.*, 2000; Meehl and Tebaldi, 2004; Schär *et al.*, 2004). These changing conditions are creating opportunities for some species to spread beyond their native ranges (Chen *et al.*, 2011) while posing a challenge to species that are currently adapted to their local environment (Holt, 1990). As sessile organisms, plants complete their life cycle in their local environment and consequently are experiencing climate conditions of increasing variability and severity. Changes in the environment during the lifetime of individual plants typically induce plastic responses in life-history traits (Bradshaw, 1965; West-Eberhard, 2003). However, simply because a given trait is plastic does not mean that this plasticity is adaptive (Ghalambor *et al.*, 2007). For example, growth plasticity may arise from an unpredictable resource limitation such as insufficient water, mineral nutrients, or light (Dorn *et al.*, 2000; van Kleunen and Fischer, 2005; Forsman, 2015). In situations where plasticity derives from resource limitation and is maladaptive or neutral for a given trait, homeostasis or lack of plasticity may, in turn, be adaptive. However, while there has been much discussion in the ecological literature about "plasticity genes" (Bradshaw, 1965; West-Eberhard, 2003; Nilson & Assmann, 2010), relatively little attention has been paid to the identification of potential "homeostasis genes."

Drought is among the strongest factors driving adaptation in plants (Siepielski *et al.*, 2017; Exposito-Alonso *et al.*, 2019). Since climate projections predict precipitation extremes to become more severe and unpredictable (Donat *et al.*, 2016), we can expect that drought episodes will become progressively more difficult for plants to adapt to. For this reason, understanding the genetic basis and adaptation potential of phenotypic traits and their plastic or homeostatic responses to drought is paramount for ameliorating climate change impacts in both natural and managed ecosystems.

The Iberian Peninsula is a drought-prone region particularly vulnerable to climate change effects on precipitation (Vicente-Serrano, 2006a; Vicente-Serrano, 2006b; Coll *et al.*, 2016; Páscoa *et al.*, 2017). The Iberian Arabidopsis population is particularly valuable because its accessions originate from a broad range of environments (Lobo *et al.*, 2001; Rey Benayas and Scheiner, 2002), and previous studies of this population have provided considerable insight into Arabidopsis evolution and development (Picó *et al.*, 2008; Montesinos *et al.*, 2009; Gomaa *et al.*, 2011; Méndez-Vigo *et al.*, 2011; Montesinos-Navarro *et al.*, 2011; Picó, 2012; Manzano-Piedras *et al.*, 2014; Wolfe and Tonsor, 2014; Vidigal *et al.*, 2016; Exposito-Alonso *et al.*, 2018a; Marcer *et al.*, 2018).

In the present study, we utilize GWAS, Transcriptome-Wide Association Studies (TWAS), and Expression Genome-Wide Association Studies (eGWAS) to identify natural genetic and transcript abundance variation underlying both plastic and homeostatic leaf area responses to drought in Iberian Arabidopsis accessions. Leaf area is a vital trait in relation to growth: leaf area production determines the total amount of light intercepted by plants, carbon assimilation, and the extent of evaporative water loss. We uncover an adaptive homeostatic growth strategy in accessions from less productive environments, dissect its genetic basis, and conclude that phenotypic homeostasis is under genetic control and of evolutionary importance, just as previously argued for plasticity.

MATERIALS AND METHODS

Plant materials and phenotyping

Seeds for 43 Iberian accessions (Table P1 for the list of accessions) were cold-stratified for four days at 4°C to synchronize germination. Plants were grown in 10 cm square pots containing Metro-mix 360 potting mixture (Sun Gro Horticulture Canada Ltd) in a greenhouse with an average daytime 500 μmol $m^{-2}s^{-1}$ photosynthetic photon flux density (PPFD) (8h light: 16h dark, with light supplied as natural daylight supplemented with 1000W metal halide lamps) and average day/night temperatures of 22 °C /20°C.

For each Iberian accession, we grew one plant per pot, with five replicates for each of control and drought treatments (10 plants for each individual accession), for a total of 430 plants (43 accessions × five control × five droughted plants). Both control and drought treatment were well-watered for the first 28 days, maintaining the soil relative water content at field capacity as measured by monitoring pot weight daily and adding water when necessary. After 28 days, plants in the drought treatment were allowed to dry down and then were rewatered to soil saturation once every ten days for a total of 14 drought cycles until the conclusion of the experiment 175 days after seeds were initially sown. Here, as in the natural environments that we sought to mimic, the soil water content was not adjusted based on the size of individual plants. Our protocol simulated the natural recurring cycle of rainfall and drought. Such cycles are often used in studies of natural variation (i.e., Exposito-Alonso *et al.*, 2018b; Exposito-Alonso *et al.*, 2019) as well as in field trials on crop cultivars (IRRI, 2021). In contrast, the well-watered treatment was maintained near field capacity throughout the experiment. Plants were spatially randomized within the greenhouse every week throughout the

experiment. At the end of the experiment, nine accessions within the drought treatment with mortality rates higher than 40% (i.e., at least two of the five replicates; Table P1) were excluded from downstream analyses.

Photographs of rosettes were taken at the time of flowering and subsequently analyzed using ImageJ (http://imagej.nih.gov/ij/) to determine the projected leaf area for each accession under both well-watered and drought treatments (Fig. S1; Table P1).

Determination of relative leaf area and plasticity

Relative leaf area (rLA) is defined here as the leaf area (LA) at the time of flowering for each accession under each experimental condition (either well-watered or drought) relative to all the accessions under the same condition. The relative leaf area of a given accession under well-watered conditions ($rLA_{i\ (well\text{-}watered)}$) is thus calculated as:

$$rLA_{i\ (well-watered)} = \frac{LA_{i\ (well-watered)}}{LA_{m\ (well-watered)}}$$

where $LA_{i\ (well\text{-}watered)}$ is the leaf area of any individual accession and $LA_{m\ (well\text{-}watered)}$ is the average of the leaf area for all accessions grown under the same conditions. Similarly, the relative leaf area under drought ($rLA_{i\ (drought)}$) for each accession is calculated as:

$$rLA_{i\ (drought)} = \frac{LA_{i\ (drought)}}{LA_{m\ (drought)}}$$

where $LA_{i\ (drought)}$ is the leaf area of any individual accession under drought and $LA_{m\ (drought)}$ is the average value for all accessions when grown under drought. A high rLA reflects greater vegetative growth of any given accession relative to the set of accessions utilized in this study. The use of rLA, rather than actual values, was essential to allow a normalized comparison of the leaf area of each accession between the watering regimes. Reaction norms based on rLA were employed to quantify plastic changes in relative leaf area between the two treatments (well-watered vs. drought). Leaf area plasticity indexes were calculated based on an established definition (Weijschedé *et al.*, 2006). The leaf area plasticity index to drought (PI) was calculated for each accession as:

$$PI = rLA_{i\ (drought)} - rLA_{i\ (well-watered)}$$

A positive leaf area plasticity index does not necessarily imply leaf area for that accession was higher under drought, but rather that under drought, a given accession displays a higher rLA relative to the rest of accessions in the study.

146

147 **Genome-wide association study**

148 Genome-Wide Association Studies (GWAS) identify genetic variants associated with natural
149 variation in a phenotypic trait of interest. We used a GWAS approach to identify polymorphisms
150 associated with natural variation in rLA and its plasticity. The online tool GWAPP
151 (http://gwas.gmi.oeaw.ac.at/) was employed using a linear regression model (Seren *et al.*, 2012). The
152 linear regression model does not address confounding effects of population stratification, family
153 structure, and cryptic relatedness (Price *et al.*, 2010); however, those issues are minimized by our
154 choice of a regional (Iberian) population (Frachon *et al.*, 2018; Tabas-Madrid *et al.*, 2018; Frachon
155 *et al.*, 2019). Nonetheless, we demonstrate that the candidate SNPs discussed here were also
156 significant after the application of a mixed model approach implemented either using GWAPP (Seren
157 *et al.*, 2012) or GWAS-Flow (Freudenthal *et al*., 2019) (Fig. S2; Tables G1-G6), providing further
158 confidence in our results.

159 We filtered out low-frequency variants (minor allele frequency (MAF) < 10%) to focus on
160 variants less likely to be undergoing negative selection or to be spurious SNPs from sequencing
161 errors. We obtained gene model annotation from the TAIR11 genome release. We defined the
162 'consensus' transcript variant as the variant producing the longest transcript. We predicted the effect
163 of every SNP using SnpEff (Cingolani *et al.*, 2012). To focus on SNPs in gene transcriptional units,
164 we subsetted the set of variants included in the untranslated regions at the 5′ and 3′ ends and the open
165 reading frames, as defined in Araport11 (Cheng *et al.*, 2017), with the potential for affecting gene
166 expression and protein composition. We also included the promoter region, defined as 5 kb upstream
167 of the most distal transcription start site. We imposed a stringent arbitrary significance threshold
168 corresponding to a score of 4 ($P < 0.0001$; Fig. S3).

169 Using the results from GWAS obtained from the association with rLA, we obtained reaction
170 norms that would reflect plastic or homeostatic patterns of genome-wide associations of these traits
171 in response to drought. The association between a phenotype and any given SNP was designated as
172 homeostatic if found significantly associated with that trait under both conditions (well-watered and
173 drought).

174

175 **Transcriptome-wide association**

176 Natural variation in gene expression is an important mechanism of local adaptation (Des Marais *et*
177 *al.*, 2012; Lasky *et al.,* 2014). Transcriptome-Wide Association Studies (TWAS) identify variation
178 in transcript abundance associated with observed variation in phenotypic traits (Gusev *et al.*, 2016;
179 Kremling *et al.*, 2019). TWAS analysis does not suffer from the limitations imposed by false non-
180 causal synthetic associations due to linkage disequilibrium (Li *et al.*, 2021) typical of GWAS (Korte
181 and Farlow 2013). Also, TWAS evaluates continuous variation in transcript abundance rather than
182 the presence/absence of SNPs with (potentially) additive effects on a continuous phenotype. We
183 retrieved the transcriptome data from rosette leaves of 727 Arabidopsis accessions from the GEO
184 dataset with accession number GSE80744 and SRA study SRP074107 (Kawakatsu *et al.*, 2016) and
185 subsetted the 35 Iberian accessions that overlapped with the 43 Iberian accessions used in our study.
186 Data wrangling was conducted utilizing the dplyr (Wickham *et al.*, 2015) and tidyr (Wickham and
187 Henry, 2018) packages. Spearman's rank correlation coefficient between individual phenotypic
188 values (relative leaf area (rLA_i), plasticity index (PI), and intrinsic water use efficiency (WUEi) from
189 Dittberner *et al.* (2018; Tables P1 and P2), and individual transcript abundance values were calculated
190 using the correlation function of the Hmisc package (Harrell Jr and Dupont, 2019). The stronger the
191 association of the two variables, the closer the Pearson correlation coefficient, r_s, will be to either +1
192 or -1. We imposed a threshold based on this correlation coefficient ($0.4 \geq |r_s| \leq 4.0$). We considered
193 this threshold to be stringent after inspection of the distribution of the results (Fig. S3). We include
194 the r_s and corresponding *P*-values in Tables T1 and T2.

195 Using the results from TWAS, we derived reaction norms to reflect homeostatic patterns of
196 transcriptome-wide associations of rLA in response to drought. Any given transcript was designated
197 homeostatic if found significantly associated with rLA (either positively or negatively; $|r_s| \geq 4.0$)
198 under both conditions (well-watered and drought).

199

200 **eGWAS**

201 Natural variation in transcript abundance can also be used to identify candidate SNPs (expression
202 SNPs or eSNPs) that control transcript abundance in an Expression Genome-Wide Association Study
203 (eGWAS). eGWAS was conducted by compiling the transcript abundance values of a given gene,
204 extracting transcript abundance for that particular gene in the 727 Arabidopsis accessions from the
205 GEO dataset with accession number GSE80744 and SRA study SRP074107 (Kawakatsu *et al.*, 2016),

206 then subsetting the 665 accessions included in the 1001 Genomes project (The 1001 Genomes
207 Consortium, 2016). Then, the online tool GWAPP (http://gwas.gmi.oeaw.ac.at/) was employed using
208 a linear regression model (Seren *et al.*, 2012) to identify candidate regulatory variants. Regulatory
209 variants are either cis or trans-acting, depending on the location of the genetic variant. cis-eSNPs
210 were defined as those located within the ORF, UTRs, or the promoter region of the regulated gene.
211 Trans-eSNPs were defined as those located within the ORF, UTRs, or promoter region of a gene
212 different from the gene transcriptionally regulated by that genetic variant.

213 **Meta-analysis of 189 Iberian Arabidopsis accessions**

214 AraCLIM (https://github.com/CLIMtools/AraCLIM) is a database that describes the local
215 environment of the Arabidopsis accessions sequenced as part of the 1001 Genomes Project (Ferrero-
216 Serrano and Assmann, 2019). We obtained from AraCLIM the values for MOD17A2 (Net Primary
217 Productivity in the spring season) (Heinsch *et al.*, 2003; Running and Zhao, 2015) at the collection
218 site of each accession and assessed correlation with rLA.

219 WUE_i is defined as the ratio between instantaneous carbon gain and transpirational water loss,
220 typically calculated per unit of leaf area (Condon *et al.*, 2002). To integrate the information from
221 previously published studies on the Iberian Arabidopsis population, we retrieved available data on
222 natural variation in intrinsic water use efficiency (WUEi, $\delta^{13}C$), previously recorded by Dittberner *et*
223 *al.* (2018), from PhenoCLIM (https://github.com/CLIMtools/PhenoCLIM) (Ferrero-Serrano and
224 Assmann, 2019). During photosynthesis, plants discriminate against $^{13}CO_2$ in the reaction center of
225 *Ribulose 1, 5-biphosphate carboxylase/oxidase* (*RuBisCO*). As stomata close, minimizing water loss
226 in response to drought, the discrimination against $^{13}CO_2$ decreases because the internal CO_2
227 concentration (C_i) becomes unavoidably reduced. As a result of their reduced C_i, plants with greater
228 WUE_i experience lower CO_2 concentrations at the sites of carboxylation (C_c) and have less negative
229 $\delta^{13}C$ values.

230 **Analyses**

231 All statistical analyses and figures were produced using R (Team, 2013). The code and data to
232 reproduce the analysis, figures, and tables are available at https://github.com/AssmannLab and
233 Zenodo. Gene Ontology (GO) biological process analysis (Tables GO1-GO10) was performed using
234 the open-source software ShinyGO v0.61: http://bioinformatics.sdstate.edu/go60/ (Ge *et al.*, 2020)

235 with the following settings: the search species was "*Arabidopsis thaliana*," the *P*-value cutoff (FDR)
236 was 0.05, and the number of most significant terms to show was ten. To replicate these results, the
237 lists of genes that were input into these analyses based on significance thresholds can be selected
238 from Tables G1-G6, T1, T2. Each analytical technique used in this study has assumptions and
239 limitations, which we discuss in Document S1.

240 **RESULTS**

241 **Natural variation in leaf area and plasticity in response to long-term cyclical drought**

242 To quantify phenotypic variation in Iberian Arabidopsis accessions exposed to drought, we conducted
243 a common garden experiment (Fig. 1a). We used image analysis to derive rosette leaf area under
244 well-watered or drought conditions (Figs. 1b, S1; Table P1). As expected, we observed a significant
245 ($P < 0.001$) reduction in leaf area resulting from drought in most genotypes, as evident from the
246 phenotypic reaction norms. In contrast, a small number of accessions exhibited constant or increased
247 leaf area under drought (Fig. 1b; Table P1), demonstrating that a reduction in leaf area in drought is
248 not inescapable. Based on these data, we calculated the relative leaf area (rLA) of each accession
249 under both well-watered and drought conditions (see Materials & Methods; Fig.1c; Table P1). We
250 used rLA rather than actual leaf area to allow comparison of the leaf area of each accession relative
251 to the study population for each watering regime. We also show that the plasticity index derived from
252 the difference in rLA between conditions (i.e. reflecting the slopes of the reaction norms in Fig. 1c;
253 Table P1) is proportional to the fold change in leaf area under drought relative to the well-watered
254 condition (Fig. S4).

255 We explored the relationship between rLA in the absence of drought and its plastic response
256 (plasticity index; PI) to drought. Figure 1d shows that accessions with higher rLA displayed greater
257 plastic reductions in rLA when subjected to drought (negative leaf area plasticity). On the contrary,
258 accessions with lower rLA under well-watered conditions displayed homeostatic phenotypic
259 responses to drought (Fig. 1d). Despite this overall trend, we also observed individual accessions with
260 high rLA under well-watered conditions and positive plasticity indexes under drought (green
261 datapoints in Fig. 1d and Fig. 1e). Conversely, a few accessions displayed low rLA and negative leaf
262 area plasticity indexes (red datapoints in Fig. 1d and Fig. 1e).

263 While the severity of drought depends on multiple environmental parameters, its
264 physiological response is very characteristic. It results in stomatal closure and a reduction in CO_2

265 assimilation, as reflected in decreases in Net Primary Productivity (NPP), an index that, therefore,
266 can be used as a reliable drought indicator (Huang *et al.*, 2016). We determined that the plastic leaf
267 area responses we observed in our study were typical of accessions from more productive habitats as
268 reflected as Net Primary Productivity in spring (NPP spring; Fig. 2a). In contrast, homeostatic leaf
269 area responses were typical of accessions from less productive habitats (Fig. 2a).

270 Genetic variants significantly associated with leaf area plasticity were identified by GWAS
271 (Fig. 2b; Table G3). Gene ontology (GO) analysis of functions associated with the genes harboring
272 the variants identified by GWAS revealed an enrichment in auxin-related processes (Table GO1).
273 Among the variants identified from GWAS (Fig. 2b; Table G3) as associated with leaf area plasticity,
274 we highlight two co-varying SNPs in the 5' and 3' UTR that comprise a haplotype of *SMALL AUXIN*
275 *UP RNA 26* (*SAUR26***,** AT3G03850) (Fig. 2c). These variants were identified by GWA analysis using
276 a linear model (Fig. 2b; Table G3). To confirm that identification of these candidates was not an
277 artifact due to population structure, we verified that these variants were also identified using two
278 different analyses that correct for population structure in the sample: Accelerated Mixed Model using
279 GWAPP and an alternative Mixed Model approach, GWAS-Flow (these two SNPs are among the
280 green datapoints in Fig. S2; see Table G3).

281 We additionally found from TWA analysis that the transcript levels of *SAUR26* are also
282 correlated with natural variation in leaf area plasticity in response to drought (Tables T1, T2).
283 eGWAS confirmed the cis-regulatory effect of these genetic variants (cis-regulation; Fig. 2d; Table
284 G6), consistent with the correlation between the genetic variation in *SAUR26*, its transcript
285 abundance, and leaf area plasticity.

286 Figure 2e illustrates the haplotypic differences in leaf area plasticity for *SAUR26* in our study.
287 Accessions harboring the minor *SAUR26* haplotype display negative plasticity in rLA, while the
288 major haplotype is associated with homeostatic and positive plasticity responses in rLA (Fig. 2e;
289 Wilcoxon P-value < 0.001). These haplotypic differences were also associated with the transcript
290 levels of *SAUR26* (Fig. 2f), which we confirmed not only in the group of accessions included in our
291 study (Wilcoxon P-value < 0.001) but also in the much larger group of 189 Iberian accessions
292 included within the 1001 Genomes Project (Fig. 2f; Wilcoxon P-value < 0.001). Both the genetic
293 variation defined by this haplotype in *SAUR26* and the resulting *SAUR26* transcript abundance are
294 associated with the interplay between plasticity and homeostasis that we determine in our study (Fig.

295 2e, f). These results highlight *SAUR26* as a candidate regulator of leaf area plasticity in response to
296 drought (Figs. 2g, h).
297 In our GWA analysis on rLA (Fig. S5a, Table G1, G2), no SNPs were associated with rLA
298 under both well-watered and drought conditions, i.e., no SNPs were associated with homeostasis and
299 thus would be depicted as horizontal lines in Fig. S5a. The results from TWA analysis were strikingly
300 different, identifying not only transcripts associated with leaf area plasticity (Fig. S5b) but also
301 transcripts associated with leaf area homeostasis (Fig. 3; Fig. S5b). Regarding homeostasis, four
302 transcripts are positively correlated with rLA under both well-watered and drought conditions:
303 *SOFL2*, *CPN60B*, *AT5G39471*, and *CKL8* (Fig. 3a). Accessions with higher transcript abundance of
304 these genes display a higher rLA under both well-watered and drought conditions (Fig. 3b-e; note the
305 similarity of the regression lines). Conversely, we identified four genes negatively correlated with
306 rLA: *RHF1A*, *AT5G60160*, *AT4G15260*, and *AT5G16800* (Fig. 3f). Accessions with a higher
307 transcript abundance of these genes display lower rLA under both well-watered and drought
308 conditions (Fig. 3g-j; note the similarity of the regression lines).
309
310 **Trade-off between plasticity and intrinsic water use efficiency**
311 It was not surprising to find a trade-off between growth and drought resistance among the accessions
312 in our study (Fig. 1d), as this is a well-established phenomenon (Zhang *et al.*, 2020). Accordingly,
313 we hypothesized that those accessions that displayed a homeostatic response to drought would exhibit
314 an increased intrinsic water-use efficiency (WUE_i), minimizing water loss. Given that $\delta^{13}C$ reflects
315 intrinsic water use efficiency (WUE_i) (Juenger *et al.*, 2005; Easlon *et al.*, 2014), we analyzed the $\delta^{13}C$
316 values recorded by Dittberner *et al.* (2018), available for 21 of the accessions used in our study. The
317 results confirm a trade-off between plasticity and WUE_i (Fig. 4a). Accessions that exhibit strong
318 negative plasticity following drought (negative leaf area plasticity indices) have a lower WUE_i in the
319 absence of drought (more negative $\delta^{13}C$ values). Those accessions that maintain or increase leaf area
320 in response to drought (positive leaf area plasticity indices) display a higher WUE_i in the absence of
321 drought (more positive $\delta^{13}C$ values).
322 GWA analysis failed to identify any genetic variants associated with the observed phenotypic
323 trade-off between intrinsic WUE_i and leaf area plasticity (Fig. 4b; Table G3, G4), i.e., no datapoints
324 in the upper right quadrant of Fig. 4b. However, TWA analysis (Fig. 4c) provided insight into this
325 trade-off. Red datapoints in Fig. 4c are transcripts with greater abundance in those negatively plastic

326 and less water-use efficient accessions depicted in red in Fig. 4a; GO analysis revealed that these
327 were enriched in processes involved in RNA modification (Table GO2); we chose the putative
328 pseudouridine synthase *CBF5* (*AT3G57150*) as an example (Figs. 4d, e). Conversely, green points in
329 Fig. 4c represent transcripts with greater abundance in the homeostatic and water-use efficient
330 accessions depicted in green in Fig. 1d. We chose *CYCLIC NUCLEOTIDE-GATED CHANNEL 16*
331 (*AT3G48010*; *CNGC16*) as an example (Figs. 4f, g).

332 We determined that in our study, accessions that in response to drought displayed either
333 increased or homeostatic leaf area plasticity also had higher WUE_i in the absence of drought (Fig.
334 4a). We then conducted a meta-analysis on the 95 Iberian accessions with published $\delta^{13}C$ information
335 (Dittberner *et al.*, 2018). GWA analysis of these accessions rendered a distinctive peak in a single
336 gene, identifying a haplotype consisting of eight co-varying SNPs in *ClpX3* (*AT1G33360*; Fig. 5a;
337 Table G5), an ATP-dependent Clp protease subunit that plays essential roles in chloroplast
338 development (Kim *et al*., 2009). Consistent with this result but more informative was the TWA
339 analysis of WUE_i in the 88 Iberian accessions with both published transcript abundance and $\delta^{13}C$
340 information (Fig. 5b): we uncovered a distinctive enrichment in photosynthesis-related genes (Fig.
341 5c; Table GO3) among transcripts that are upregulated among accessions with high WUE_i (more
342 positive $\delta^{13}C$ values; Fig. 5b; Fig. S6; Table T1, T2). We highlight the positive relationships with
343 WUE_i uncovered for the transcript abundance of *RuBisCO small subunit 2B* (*AT5G38420*; *RBCS2B;*
344 Fig. 5d) and the positive relationship between the transcript abundance of *SAUR26* and WUE_i (Fig.
345 5e), in concordance with other findings in our study.
346
347 **DISCUSSION**
348
349 **Identifying candidate regulators of plasticity and homeostasis**
350 An adaptive trade-off between growth and drought resistance in plants is well-established (Zhang *et*
351 *al.*, 2020). In productive environments, accessions with higher rLA in the absence of drought may
352 have an advantage in competing for aboveground resources relative to smaller individuals, as
353 proposed by Tilman (1988). On the other hand, plants adapted to unproductive environments typically
354 fix less carbon, have higher WUE_i, and display reduced vegetative growth, even when grown in rich
355 environments (Parsons, 1968; Chapin, 1991); however, these plants are typically stress-tolerant
356 (Billings and Mooney, 1968; Grime, 1977). In our study, accessions typical of more productive areas

357 display strong and negative plastic responses to drought (Fig. 2a). Conversely, accessions with
358 homeostatic or even positive plasticity in rLA in response to drought typify less productive areas (Fig.
359 2a). Here, we sought to identify the genetic basis of these contrasting ecological strategies.

360 Our main interest was not to identify natural variation associated with well-watered or drought
361 phenotypes, but rather natural variation associated with the degree of plasticity evoked in response to
362 drought, i.e., natural variation associated with reaction norms, rather than with phenotypes in one
363 environment or the other (well-watered or drought). In exploring the genetic basis of plasticity, we
364 identified 31 genes corresponding to the top 50 candidate SNPs with the strongest association with
365 the leaf area plasticity index (Figure 2b; Table 1; Table G3). To the best of our knowledge, 20 out of
366 these 31 genes have been previously characterized, and many of these are related to auxin regulation
367 and leaf expansion. This enrichment in auxin-related processes was confirmed by GO analysis (Table
368 GO1). Notably, when we compare the candidates resulting from GWA analysis on rLA vs. leaf area
369 plasticity, only eight candidate SNPs overlapped between both traits (green datapoints in Figure S7a),
370 and none of these eight SNPs are in genes related to auxin. In other words, the auxin-related candidate
371 genes are related to *plasticity* in this trait and not to the trait itself.

372 The variant with the strongest association with the plastic response to drought was the auxin
373 efflux carrier family protein *PIN8* (*AT5G15100*). Among the associated SNPs, we also found two co-
374 varying SNPs in *AUXIN RESPONSE FACTOR 16* (*ARF16*; *AT4G30080),* two co-varying SNPs in
375 *SMALL AUXIN UP RNA 26* (*SAUR26*; *AT3G03850*); two variants in *AGAMOUS-like 15*
376 (*AT5G13790*; *AGL15*), a gene that negatively regulates auxin signaling in Arabidopsis (Zheng *et al.*,
377 2016); and three variants in *LONESOME HIGHWAY LIKE 1* (*LL2*; *AT2G31280*), an atypical basic
378 helix-loop-helix (bHLH) transcription factor that regulates early xylem development downstream of
379 auxin (Ohashi-Ito *et al.*, 2013).

380 Among the candidates that are not formally included in the GO category "response to auxin,"
381 we found six co-varying SNPs in the abscisic acid receptors *PYR1-like 11* (*PYL11*; *AT5G45860*) and
382 *PYR1-like 12* (*PYL12*; *AT5G45870*). ABA and auxin pathways interact in the regulation of growth
383 (Emenecker & Strader 2020), and also in the regulation of plasma membrane H^+ ATPases (of which
384 there is one member in the list, *H^+ ATPase 2* (*AHA2; AT4G30190*)) during cell expansion (Spartz *et*
385 *al.,* 2014) and stomatal control (Wong *et al*., 2021). We also found four co-varying SNPs in the *Basic*
386 *helix-loop-helix (bHLH) DNA-binding family protein MYC3* (*AT5G46760*), a known regulator of
387 glucosinolate biosynthesis (Schweizer *et al.*, 2013). Auxin negatively regulates glucosinolate levels,

388 which appears to integrate growth and stomatal regulation during drought (Salehin *et al.*, 2019). GO
389 biological process analysis on positively correlated candidates resulting from TWAS analysis on leaf
390 area plasticity index for drought also revealed an enrichment of glucosinolate biosynthesis genes
391 (Table GO4).

392 We found that among the auxin-related variants associated with leaf area plasticity (Fig. 2b),
393 SNPs in *SAUR26* were of particular interest. The majority of characterized *SAUR* genes are positive
394 regulators of plant growth (Spartz *et al.*, 2014; Li *et al.*, 2015; Stortenbeker and Bemer, 2019). The
395 two associated variants in *SAUR26* were found in the 5' and 3' UTR, respectively (Fig. 2c), regions
396 of the transcript that typically regulate gene expression. Indeed, we found the transcript levels of
397 *SAUR26* to be associated with the genetic variation in *SAUR26* itself (cis-regulation; Fig. 2d), which
398 we confirmed both in the group of accessions included in this study, and importantly, in the larger
399 group of 189 Iberian accessions in the 1001 Genomes Project (Fig. 2f). The minor haplotype is
400 associated with negative plasticity in leaf area in response to drought. Conversely, the major
401 haplotype, associated with higher transcript abundance of *SAUR26*, is associated with leaf area
402 homeostasis and positive plastic responses (Fig. 2e).

403 Natural variation in transcript abundance of *SAUR26* explained 18% of the observed plastic
404 response in leaf area to drought in our study (Fig. 2g, h). The importance of *SAUR26* is supported by
405 previous work that revealed natural genetic variation in *SAUR26* associated with growth thermo-
406 responsiveness of the rosette compactness index (Wang *et al.*, 2019), and cis-elements in the 5'
407 upstream region or the 3'UTR region of *SAUR26* that were responsible for this response (Wang *et al.*
408 2021). This conclusion is also supported by our meta-analysis of the larger Iberian population with
409 transcriptome data, which also identified *SAUR26* transcript abundance as positively correlated with
410 higher WUE_i (Fig. 5b, e), along with other related auxin-related transcripts such as *AUXIN*
411 *RESISTANT 3* (*AXR3*, also known as *IAA17*, *AT1G04250;* Fig. S6a) (Leyser *et al.*, 1996) and *SMALL*
412 *AUXIN UPREGULATED 15* (*SAUR15*, *AT4G38850*; Fig. S6b) (Oh *et al.*, 2014) (Fig. 5b). As we
413 uncover in this study, both transcript abundance and natural genetic variation in *SAUR26* cis-
414 regulatory elements are associated with the interplay between plasticity and homeostasis in rLA
415 following drought stress (Fig. 2, Tables G3, T1, T2).

416 Interestingly, the minor haplotype frequency for this *SAUR26* haplotypic variant in our study
417 sample (minor haplotypic frequency, MHF = 38.09%) is similar to the frequencies we find in the 189
418 accessions within the Iberian population (MHF = 35.98%). However, the minor haplotype in the

419 Iberian population becomes the haplotype in higher frequency (64.14%) in the global 1001 Genomes
420 collection. It has been shown that Iberian Arabidopsis populations locally adapted to drought
421 conditions in this region out-perform accessions from wetter areas of Northern Europe when both are
422 exposed to drought (Exposito-Alonso *et al.*, 2019). Following this, given that the major haplotype in
423 our study is associated with homeostatic responses to drought (Fig. 2e) and that its frequency becomes
424 reduced outside the drought-prone Iberian region, we can speculate that this *SAUR26* haplotypic
425 variant is under selection in the Iberian population, conferring an adaptive advantage to the water-
426 limited conditions of the region.
427 We did not identify any SNPs associated with rLA under both well-watered and drought
428 conditions. Therefore, the genetic basis of growth homeostasis under drought could not be defined in
429 our study using GWAS (Fig. S5a). On the other hand, the reaction norms based on the strength of
430 association of transcript abundance with rLA, i.e., TWAS, identify four transcripts that are positively
431 correlated with rLA under both well-watered and drought conditions (Fig. 3a-e). This means that
432 accessions with greater transcript abundance for those genes display higher rLA under both well-
433 watered and drought conditions. Conversely, we identified four transcripts negatively correlated with
434 rLA such that accessions with a higher transcript abundance of those genes display lower rLA under
435 both well-watered and drought conditions (Fig. 3f-j). Therefore, these eight genes are strong
436 functional candidates for the homeostatic regulation of rLA.
437 Of the eight resultant candidate genes, most have not been characterized, and for those that
438 have, their function is not necessarily known to be involved in growth processes regulating leaf area,
439 suggesting that further research is needed regarding the functional roles of these genes and how they
440 contribute to homeostasis.
441
442 **Trade-off between relative leaf area (rLA), plasticity and WUE_i**
443 Plant species with low relative growth rates exhibit high WUE_i (Angert *et al.*, 2009; Kimball *et al.*,
444 2012). We can hypothesize that those plants with lower growth rates will have better drought
445 resistance, consequently displaying growth homeostasis. These observations are both consistent with
446 results from classic ecological studies and confirmed in crop cultivars (Kasuga *et al.*, 1999; Ferrero-
447 Serrano and Assmann, 2016; Ferrero-Serrano *et al.*, 2018). In our study, accessions with lower rLA
448 and homeostatic responses to drought display a greater abundance of transcripts encoding functions
449 related to ion transport (yellow datapoints in Fig. S7b; Tables T1, T2, GO5), which could be related

450 to osmoregulation and stomatal control of transpiration. Consistent with this argument, the
451 homeostatic response in rLA in response to prolonged drought that we observe in our study correlates
452 positively with a high predicted WUE_i recorded by Dittberner *et al.* (2018) for the same accessions
453 (Fig. 4a).

454 We then studied the genetic basis of this trade-off between rLA, plasticity, and WUE_i. There
455 were no SNPs associated with both the leaf area plasticity index and WUE_i (Fig. 4b). However, when
456 we compare the candidates obtained from TWA analysis, we identify transcripts associated with both
457 low WUE_i and a negative plastic response in leaf area following sustained drought (Fig. 4c).
458 Conversely, we identify a set of transcripts that is significantly associated with both leaf area
459 homeostasis (more positive leaf area plasticity index) and increased WUE_i (Fig. 4c). To exemplify
460 these opposed responses to drought, given the enrichment in RNA modification and ion transport
461 genes that we found in the transcripts regulating the trade-off between relative leaf area and plasticity
462 (Fig S7b; Tables T1, T2), we highlight two of the genes identified by TWAS, with opposite
463 correlations between transcript abundance and relative leaf area plasticity (Figs. 4d, e vs. Figs 4f, g):
464 (*CBF5*; *AT3G57150*) and *CYCLIC NUCLEOTIDE GATED CHANNEL 16* (*CNGC16*; *AT3G48010*).

465 *CBF5* encodes a protein with homology to a category of pseudouridine synthases, and its
466 knockout in Arabidopsis is lethal (Lemontova *et al.,* 2007). Originally only non-coding RNAs,
467 particularly rRNAs, were thought to be pseudouridylated, but it is now recognized that mRNAs are
468 also a target for pseudouridylation. In both yeast and human cells, this post-transcriptional
469 modification is induced by heat shock, with consequent impacts on splicing, mRNA stability, and
470 translation (Karijolich *et al*., 2015). We observe that accessions with higher transcript abundance of
471 *CBF5* display both strong negative plastic responses in rLA in response to drought (Fig. 4d) and
472 reduced WUE_i (Fig. 4e). Our observations suggest that stress-induced pseudouridylation may also
473 occur in plants, with functional consequences for drought tolerance; other types of mRNA
474 modifications in plants have been correlated with increased mRNA stability and translation under
475 salinity stress (Kramer et al., 2020) and improved heat tolerance (Tang *et al.,* 2020).

476 Conversely, transcript abundance of *CNGC16* is associated with homeostatic responses in
477 rLA and increased WUE_i. CNGCs are a superfamily of ion channels permeable to divalent and
478 monovalent cations (Köhler *et al.*, 1999; DeFalco *et al.*, 2016). *CNGC*s like *CNGC5* and *CNGC6*
479 have been reported to be the basis of a cyclic GMP (cGMP)-activated nonselective Ca^{2+}-permeable
480 cation channel activity in the plasma membrane of Arabidopsis guard cells (Wang *et al.*, 2013)

481 associated with stomatal closure. *CNGC16* is also critical for reproductive success following drought
482 stress (Tunc-Ozdemir *et al.*, 2013). Consistent with these functional roles, in our study, higher
483 transcript abundance of *CNGC16* is found in accessions with positive leaf area plasticity indexes
484 under drought (leaf area homeostasis; Fig. 4f); and with high WUE_i (Fig. 4g).

485 Given the increased plastic responses in leaf area found in accessions with lower WUE_i, we
486 next conducted a meta-analysis on the larger set of 95 Iberian accessions with $\delta^{13}C$ information from
487 a previous study focused on the global Arabidopsis population (Dittberner *et al.*, 2018). We identified
488 a distinctive peak consisting of eight co-varying SNPs in a single gene, *ClpX3* (*AT1G33360*; Fig. 5a),
489 an ATP-dependent Clp protease subunit (Nishimura and van Wijk, 2015). Null mutants in a different
490 chloroplast protease subunit, ClpR, display a remarkable loss of chlorophyll (95 to 98% reduction)
491 and photosynthetic capacity, turning entirely white when grown under high light (Kim *et al.*, 2009).

492 TWA analysis of WUE_i determined from $\delta^{13}C$ values in the 88 Iberian accessions with both
493 $\delta^{13}C$ information (Dittberner *et al.*, 2018) and published transcript abundance (Kawakatsu *et al.*,
494 2016) further supported the relationship with photosynthesis. Our TWAS on WUE_i in the larger
495 Iberian population identified 31 out of the 45 candidate genes for WUE_i that we also identified in the
496 subset of 20 Iberian accessions in our experimental study for which published $\delta^{13}C$ data were
497 available (Table T1 and T2). Gene Ontology (GO) biological process analysis of the resultant 45
498 candidates positively correlated with $\delta^{13}C$ uncovered an unequivocal enrichment in photosynthesis-
499 related genes for transcripts that are upregulated in accessions with high WUE_i (less negative $\delta^{13}C$
500 values; Figs. 5b, 5c; Table GO3). Among the candidates from our TWA analysis that are positively
501 related to WUE_i was *RuBisCO small subunit 2B* (*AT5G38420*; *RBCS2B;* Fig. 5d). An upregulation
502 in *RuBisCO* may compensate for suboptimal CO_2 concentrations at the sites of carboxylation arising
503 from reduced stomatal apertures in plants from drought-prone environments. We illustrate eight
504 additional genes with transcript abundances that were positively associated with WUE_i in Fig. S6.
505 Among these are *NADH dehydrogenase-like complex M* (*NdhM*, *AT4G37925;* Fig. S6c), required for
506 *NdH* complex assembly (Ifuku *et al.*, 2011), and *High cyclic electron flow 1* (*HCEF1*; *AT3G54050*;
507 Fig. S6d)) (Livingston *et al.*, 2010), both regulators of cyclic electron flow around PSI (Yamori *et*
508 *al.*, 2011), *ATP-Synthase δ-Subunit* (*ATPD*, *AT4G09650*; Fig. S6e) (Maiwald *et al.*, 2003),
509 *Photosystem I reaction center subunit PSI-N* (*PSAN*, *AT5G64040;* Fig. S6f) (Haldrup *et al.*, 1999),
510 and *Photosystem II subunit O-2* (*PSBO2*; *AT3G50820;* Fig. S6g) (Murakami *et al.*, 2005). Also, the
511 candidate with the highest association score is a member of the plasma membrane intrinsic protein

512 (PIP) subfamily of aquaporins (*PIP1;5*; *AT4G23400*; Fig. S6h). PIPs regulate water flux in guard
513 cells as well as membrane permeability to CO_2 in the mesophyll, with an important effect on
514 mesophyll conductance and CO_2 concentration at the sites of carboxylation (C_c) (Groszmann *et al.*,
515 2017). Thus, *PIP1;5* is also a candidate regulator of photosynthetic rates. As discussed before,
516 *SAUR26* is also among these candidates (Fig. 5b, e), increasing our confidence in the role of this gene
517 as a regulator of plastic responses to drought (Fig. 2).

518 Among the candidates that are negatively related to high WUE_i there is an enrichment in
519 carbohydrate transport-related processes (Table GO6). We can speculate that this enrichment reflects
520 the transport of carbohydrates produced during photosynthesis to promote plant growth. This would
521 be concordant with the trade-off between growth and WUE_i that we observe in our study.

522

523 **Conclusions**

524 The adaptive role of plasticity has been at the center of a long-standing debate. Much work and
525 discussion have focused on the principle that if indeed plasticity is adaptive, it may be under genetic
526 control (Bradshaw, 1965; Via *et al.*, 1995); however, few relevant genes have been identified. Here
527 we propose that not only plasticity but also homeostasis is under genetic control and subject to natural
528 selection. This concept is supported by our dissection of the genetic basis of both plasticity and
529 homeostasis in leaf area following drought, which identifies specific genes implicated in each
530 process.

531 Knowledge from natural populations of how plants adapt to their environment can be
532 incorporated in breeding and biotechnological approaches to crop improvement. In this study, we
533 observe a trade-off between growth and drought response. A similar trade-off between stress
534 tolerance and productivity threatens food security. It is noteworthy that we also found accessions that
535 did not display this trade-off, e.g., those accessions marked in green in Fig. 1d,e. These accessions
536 may be of particular interest from an agronomic perspective.

537 The concerted use of TWAS and GWAS increases the power to link genes to phenotypes
538 (Kremling et al., 2019). A similarly integrative approach has identified water use efficiency traits in
539 sorghum (Ferguson et al., 2020). Here, this approach has yielded insights into the genetic basis of
540 response to resource limitation, identifying both candidate "plasticity genes" and candidate
541 "homeostasis genes" for further study. In particular, the identification of potential homeostatic
542 mechanisms has important implications for maintaining crop yield in the face of climate change.

543 Results arising from diverse genome-wide analyses in both model and crop species (Schindele et al.,
544 2020) can now be used to inform powerful new CRISPR-based approaches for gene editing and
545 modulation of transcript abundance toward crop improvement (Abudayyeh et al., 2017).
546
547 **Supporting information**
548
549 The following supplemental materials are available
550 **Figure S1.** Rosette leaf area observations at the time of flowering (Table P1).
551 **Figure S2.** The use of different GWAS methods improves confidence in candidates for leaf area
552 plasticity and WUE_i.
553 **Figure S3.** Histograms of the distribution of r_s and scores obtained from GWA and TWA analyses of
554 the traits discussed in this study illustrate the stringent significance thresholds imposed in this study.
555 **Figure S4.** The plasticity index that we calculated is predictive of the fold change in leaf area under
556 drought relative to well-watered conditions.
557 **Figure S5.** Genotypic and transcriptomic reaction norms based the strength of association of
558 individual SNPs and transcripts highlight the variation of these associations depending on water
559 availability.
560 **Figure S6.** Illustration of transcript variants that regulate intrinsic water use efficiency in Iberian
561 Arabidopsis accessions.
562 **Figure S7.** TWAS identifies the genetic basis of the trade-off between relative leaf area (rLA) and
563 its plastic response to drought.
564 **Table P1.** Leaf area measurements recorded in this experiment (well-watered & drought). Calculated
565 relative leaf area (rLA) and plasticity, water use efficiency (WUE_i, $\delta^{13}C$) values recorded by
566 Dittberner *et al.* (2018) and MOD17A2 net primary productivity) information obtained from
567 AraCLIM (Ferrero-Serrano & Assmann, 2019) for the accessions included in our study.
568 **Table P2.** Water use efficiency (WUEi, $\delta^{13}C$) values recorded by Dittberner *et al.* (2018) for 95
569 Iberian Arabidopsis accessions.
570 **Table G1.** Candidates obtained from GWAS on relative leaf area (rLA) under well-watered
571 conditions. Only associations with a score ≥ 4 are included here. For a raw, unfiltered, as well as for
572 a fully filtered and annotated (see Materials & Methods) version of this GWAS output, please visit
573 the data repository.

574 **Table G2.** Candidates obtained from GWAS on relative leaf area (rLA) under drought. Only
575 associations with a score ≥ 4 are included here. For a raw, unfiltered, as well as for a fully filtered
576 and annotated (see Materials & Methods) version of this GWAS output, please visit the data
577 repository.
578 **Table G3.** Candidates obtained from GWAS on leaf area plasticity. Only associations with a score ≥
579 4 are included here. For a raw, unfiltered, as well as for a fully filtered and annotated (see Materials
580 & Methods) version of this GWAS output, please visit the data repository.
581 **Table G4.** Candidates obtained from GWAS on water use efficiency (WUEi, δ13C) values recorded
582 by Dittberner *et al.* (2018) for the accessions included in our study. Only associations with a score ≥
583 4 are included here. For a raw, unfiltered, as well as for a fully filtered and annotated (see Materials
584 & Methods) version of this GWAS output, please visit the data repository.
585 **Table G5**. Candidates obtained from GWAS on water use efficiency (WUEi, δ13C) values recorded
586 by Dittberner *et al.* (2018) for 95 Iberian Arabidopsis accessions. For a raw, unfiltered, as well as for
587 a fully filtered and annotated (see Materials & Methods) version of this GWAS output, please visit
588 the data repository.
589 **Table G6.** Candidates obtained from eGWAS on the natural variation in transcript abundance of
590 SAUR26 extracted from Kawakatsu *et al.* (2016). For a raw, unfiltered, as well as for a fully filtered
591 and annotated (see Materials & Methods) version of this GWAS output, please visit the data
592 repository.
593 **Table T1**. Results from TWAS (r_s).
594 **Table T2.** Results from TWAS (*P*-value).
595 **Table GO1.** GO analysis on the 31 genes corresponding to the top 50 candidate SNPs resulting from
596 GWAS analysis on leaf area plasticity index for drought.
597 **Table GO2.** GO analysis on the 58 genes identified from TWAS to exhibit transcript abundances
598 that are negatively correlated with leaf area plasticity index for drought, and negatively correlated
599 with water use efficiency determined from ($\delta^{13}C$) values from accessions overlapping with our sample
600 (red datapoints in 4C).
601 **Table GO3.** GO analysis on the 45 genes identified from TWAS to exhibit transcript abundances
602 that are positively correlated with water use efficiency determined from ($\delta^{13}C$) values in 88 Iberian
603 Arabidopsis accessions (datapoints with $r_s \geq 0.4$ in Figure 5b).

604 **Table GO4.** GO analysis on the 494 genes identified from TWAS to exhibit transcript abundances
605 that are positively correlated with leaf area plasticity index for drought (green and grey datapoints
606 with $r_s \geq 0.4$ in the y-axis representing leaf area plasticity index in Figure 4c).
607 **Table GO5.** GO analysis on the 28 genes identified from TWAS to exhibit transcript abundances
608 that are negatively correlated with relative leaf area (rLA) under well-watered conditions, and
609 positively correlated with leaf area plasticity index for drought (blue datapoints in S7b).
610 **Table GO6.** GO analysis on the 11 genes identified from TWAS to exhibit transcript abundances
611 that are negatively correlated with water use efficiency determined from ($\delta^{13}C$) values in 88 Iberian
612 Arabidopsis accessions (datapoints with $r_s \leq -0.4$ in Figure 5b).
613 **Table GO7.** GO analysis on the 302 genes identified from TWAS to exhibit transcript abundances
614 that are positively correlated with relative leaf area (rLA) under drought.
615 **Table GO8.** GO analysis on the 134 genes identified from TWAS to exhibit transcript abundances
616 that are negatively correlated with relative leaf area (rLA) under well-watered conditions (blue and
617 grey datapoints with $r_s \leq 0.4$ in the x-axis of Figure S7b).
618 **Table GO9**. GO analysis on the 177 genes identified from TWAS to exhibit transcript abundances
619 that are positively correlated with relative leaf area (rLA) under well-watered conditions (yellow and
620 grey datapoints with $r_s \geq 0.4$ in the x-axis of Figures S7b representing).
621 **Table GO10.** GO analysis on the 233 genes identified from TWAS to exhibit transcript abundances
622 that are negatively correlated with relative leaf area (rLA) under drought.
623

Tables

Table 1. List of 31 genes corresponding to the top 50 candidate SNPs with the strongest association with the leaf area plasticity index. Genes encoding proteins with auxin-related functions from GO analysis are bolded; additional genes related to auxin based on literature analysis are underlined.

Chr	Position	MAF (%)	Gene ID	Gene description	Label
5	**4892996**	**38.24**	***AT5G15100***	***Auxin efflux carrier family protein***	***PIN8***
3	1787622	26.47	*AT3G05970*	*long-chain acyl-CoA synthetase 6*	*LACS6*
4	**14703801**	**26.47**	***AT4G30080***	***auxin response factor 16***	***ARF16***
4	**14705049**	**26.47**	***AT4G30080***	***auxin response factor 16***	***ARF16***
5	5238732	23.53	*AT5G16030*	*mental retardation GTPase activating protein*	*AT5G16030*
3	975320	32.35	*AT3G03810*	*O-fucosyltransferase family protein*	*EDA30*
3	970856	20.59	*AT3G03800*	*syntaxin of plants 131*	*SYP131*
5	15293597	26.47	*AT5G38280*	*PR5-like receptor kinase*	*PR5K*
5	15293610	26.47	*AT5G38280*	*PR5-like receptor kinase*	*PR5K*
5	15293481	41.18	*AT5G38280*	*PR5-like receptor kinase*	*PR5K*
4	14691629	35.29	*AT4G30060*	*Core-2/I-branching beta-1,6-N-acetylglucosaminyltransferase family protein*	*AT4G30060*
5	4659907	35.29	*AT5G14450*	*GDSL-like Lipase/Acylhydrolase superfamily protein*	*AT5G14450*
5	18974632	20.59	*AT5G46760*	*Basic helix-loop-helix (bHLH) DNA-binding family protein*	*MYC3*
5	18974915	20.59	*AT5G46760*	*Basic helix-loop-helix (bHLH) DNA-binding family protein*	*MYC3*
5	18975625	20.59	*AT5G46760*	*Basic helix-loop-helix (bHLH) DNA-binding family protein*	*MYC3*
5	18975826	20.59	*AT5G46760*	*Basic helix-loop-helix (bHLH) DNA-binding family protein*	*MYC3*
3	**983189**	**38.24**	***AT3G03850***	***SAUR-like auxin-responsive protein family***	***SAUR26***
3	**983517**	**38.24**	***AT3G03850***	***SAUR-like auxin-responsive protein family***	***SAUR26***
3	1798927	29.41	*AT3G05990*	*Leucine-rich repeat (LRR) family protein*	*AT3G05990*
5	4433730	29.41	*AT5G13740*	*zinc induced facilitator 1*	*ZIF1*
5	4433740	29.41	*AT5G13740*	*zinc induced facilitator 1*	*ZIF1*
5	4436472	29.41	*AT5G13740*	*zinc induced facilitator 1*	*ZIF1*
5	4436745	29.41	*AT5G13740*	*zinc induced facilitator 1*	*ZIF1*
5	4442005	29.41	*AT5G13760*	*Plasma-membrane choline transporter family protein*	*AT5G13760*
5	**4450177**	**29.41**	***AT5G13790***	***AGAMOUS-like 15***	***AGL15***
5	**4450180**	**29.41**	***AT5G13790***	***AGAMOUS-like 15***	***AGL15***
2	13323264	23.53	*AT2G31260*	*autophagy 9*	*APG9*
2	13330862	23.53	*AT2G31270*	*CDT1-like protein A*	*CDT1A*
2	13341047	23.53	*AT2G31280*	*transcription factor bHLH155-like protein*	*LL2*
2	13341186	23.53	*AT2G31280*	*transcription factor bHLH155-like protein*	*LL2*
2	13342866	23.53	*AT2G31280*	*transcription factor bHLH155-like protein*	*LL2*
2	13343940	23.53	*AT2G31290*	*Ubiquitin carboxyl-terminal hydrolase family protein*	*AT2G31290*
2	13345229	23.53	*AT2G31290*	*Ubiquitin carboxyl-terminal hydrolase family protein*	*AT2G31290*
2	13345701	23.53	*AT2G31290*	*Ubiquitin carboxyl-terminal hydrolase family protein*	*AT2G31290*
2	13346191	23.53	*AT2G31300*	*actin-related protein C1B*	*ARPC1B*
2	13358923	23.53	*AT2G31320*	*poly(ADP-ribose) polymerase 2*	*PARP1*
3	22329843	23.53	*AT3G60400*	*Mitochondrial transcription termination factor family protein*	*SHOT1*
4	14775183	32.35	*AT4G30190*	*H[+]-ATPase 2*	*AHA2*
4	6154596	32.35	*AT4G09770*	*TRAF-like family protein*	*AT4G09770*
1	29310771	20.59	*AT1G77960*	*repressor ROX1-like protein*	*AT1G77960*
5	18596240	20.59	*AT5G45840*	*Leucine-rich repeat protein kinase family protein*	*AT5G45840*
5	18604234	20.59	*AT5G45860*	*PYR1-like 11*	*PYL11*
5	18606400	20.59	*AT5G45870*	*PYR1-like 12*	*PYL12*
5	18606524	20.59	*AT5G45870*	*PYR1-like 12*	*PYL12*
5	18606721	20.59	*AT5G45870*	*PYR1-like 12*	*PYL12*
5	18606940	20.59	*AT5G45870*	*PYR1-like 12*	*PYL12*
5	18606953	20.59	*AT5G45870*	*PYR1-like 12*	*PYL12*
5	**18613579**	**20.59**	***AT5G45890***	***senescence-associated gene 12***	***SAG12***
5	3708088	20.59	*AT5G11550*	*ARM repeat superfamily protein*	*AT5G11550*
5	4655788	20.59	*AT5G14430*	*S-adenosyl-L-methionine-dependent methyltransferases superfamily protein*	*AT5G14430*

629 **Figures**

630 **Figure 1. Arabidopsis rosette leaf area observations**. **(a)** Detail of the common garden experiment,
631 illustrating the randomization of well-watered and drought treatments, as reflected in soil coloration.
632 **(b)** Phenotypic reaction norms illustrating a reduction of leaf area in response to drought in most but
633 not all accessions. Violin distributions represent probability densities of leaf area (cm^2) among the
634 accessions included in this study. Datapoints depict the mean phenotypic values of individual
635 accessions, and the reaction norms represent the plastic response in the leaf area of each accession in
636 response to drought (t-test; *P*-value < 0.001). **(c)** Phenotypic reaction norms illustrating plastic and
637 homeostatic responses in relative leaf area (rLA). Violin distributions represent probability densities
638 of rLA among the accessions included in this study. Datapoints depict the rLA of individual
639 accessions, and the reaction norms represent the plastic response in rLA of each accession in response
640 to drought (t-test; *P*-value > 0.05). **(d)** Negative relationship (*P*-value < 0.05) between leaf area
641 plasticity index (slope of the reaction norms in 1c) in response to drought (y-axis) and rLA under
642 well-watered conditions (x-axis). Data were fitted using a linear regression model. Grey shadow
643 represents the 95% CI of the fit regression line. Four different quadrants are defined by two dashed
644 lines: the average rLA (x-axis), and y = 0, which is the homeostatic point at which a change in water
645 availability does not affect rLA (i.e. a plasticity index of 0). Data points depict individual accessions
646 with their respective label. Data points are colored based on in which quadrant they fall (see text).
647 **(e)** Images illustrating the plastic and homeostatic responses to drought found among the accessions
648 included in this study.

649 **Figure 2. *SMALL AUXIN UP RNA 26* (*SAUR26,* AT3G03850) is a candidate regulator of**
650 **Arabidopsis leaf plasticity in response to drought. (a)** Accessions from more productive areas
651 display stronger negative reductions in leaf area plasticity relative to accessions from less productive
652 environments. Scatter plot depicting the negative relationship (*P*-value < 0.05) between leaf area
653 plasticity index (y-axis) and Net Primary Productivity during the spring season (x-axis). **(b)**
654 Manhattan plot representing the strength of association between genetic variants and leaf area
655 plasticity in response to drought. **C.** *SAUR26* gene model, including the two co-varying SNPs
656 highlighted in 2b. Orange block depicts the sole exon, green block the 5' UTR, dark green block the
657 3' UTR. Labels above indicate the position of the two SNPs that co-vary, forming a haplotype in our
658 sample. Major/minor allele frequency in our sample, in the 189 accessions from the Iberian Peninsula

659 included in the 1001 Genome Project, and in the whole 1001 Genomes Project sample dataset is
660 provided. **(d)** Manhattan plot representing the genome-wide strength of association between the
661 genetic variation present within the 665 accessions from the transcript abundance reference panel
662 (Kawakatsu *et al.*, 2016) that overlap with the collection of accessions included in the 1001 Genomes
663 Project, and the variation in the transcript abundance of *SAUR26* (Kawakatsu *et al.*, 2016). The peak
664 in chromosome 3 represents the cis-genetic variants in *SAUR26* affecting its transcript abundance.
665 For the Manhattan plots in 2**b** and **e**, the score (y-axis) consists of the negative logarithm of the *P*-
666 value and provides association strength. Each data point represents a SNP with a color corresponding
667 to the chromosome where the genetic variants are located. The x-axis and the different colors shown
668 in the SNPs depicted in the Manhattan plots represent the different chromosomes. The higher the
669 score, the lower the *P*-value, and the stronger the association between genetic variation and leaf area
670 plasticity or *SAUR26* transcript abundance. **(e)** The major haplotype of *SAUR26* is associated with
671 homeostatic or positive responses of relative leaf area (rLA) in response to drought. Conversely, the
672 minor haplotype is associated with plastic responses in rLA in response to drought. Violin plots show
673 significantly different probability densities of leaf area plasticity in response to drought for the major
674 and minor allele haplotypes in *SAUR26.* **(f)** The haplotypes in *SAUR26* associated with leaf area
675 plasticity/homeostasis in response to drought are associated with difference in *SAUR26* gene
676 expression. Violin plots show significantly different probability densities of *SAUR26* transcript
677 abundance for the major and minor allele haplotypes in *SAUR26* for both our sample and the entire
678 Iberian population. **(g)** Scatter plot illustrating the positive relationship between leaf area plasticity
679 index (y-axis) and *SAUR26* transcript abundance (x-axis). For **2**a and **2g**, the grey shadow represents
680 the 95% CI of the fit regression line (dark grey). **(h)** Cartoon illustrating the regulatory role of genetic
681 and transcript variation in *SAUR26* and the response of leaf area to drought.

682 **Figure 3. Transcriptomic reaction norms uncover genetic correlates of Arabidopsis leaf area**
683 **homeostasis in response to drought. (a**) homeostatic reaction norms for transcripts significantly and
684 positively correlated with relative leaf area (rLA) under both watering regimes. (b) to (e). Scatter
685 plots illustrating positive and homeostatic relationships (*P*-value < 0.05) between rLA under both
686 well-watered (closed circles) and drought conditions (open circles) conditions (y-axis), and transcript
687 abundance (FPKM; x-axis) of **(b)** AT5G39471, **(c)** *SOB FIVE-LIKE 2* (*SOFL2; AT1G68870*)**, (d)**
688 *CHAPERONIN 60 BETA* (*CPN60B*; *AT1G55490*), and **(e)** *CASEIN KINASE I-LIKE 8* (*CKL8*;
689 *AT5G43320*). **(f)** homeostatic reaction norms for transcripts significantly and negatively correlated

690 with rLA under both watering regimes. (g) to (j) Scatter plots illustrating negative and homeostatic
691 relationships (*P*-value < 0.05) between rLA under both well-watered (closed circles) and drought
692 conditions (open circles) (y-axis), and transcript abundance (FPKM; x-axis) of **(g)** AT5G60160, (**h)**
693 *AT4G15260***, (i)** *AT5G16800*, and **(j)** *RING-H2 GROUP F1A* (*RHF1A*; *AT4G14220*). For 3a and 3f,
694 Spearman's rank correlation coefficient ($r_{s;}$ y-axis) indicates the correlation between the rLA and the
695 natural variation in transcript abundance of each gene. In figures b to e and g-j, data were fitted using
696 a linear regression model. Also, in panels b-e and g-j, filled circles depict the rLA of accessions grown
697 under well-watered conditions, while empty circles squares depict the rLA of accessions grown under
698 drought.
699

700 **Figure 4. Arabidopsis accessions that display leaf area homeostasis in response to drought,**
701 **display higher water use efficiency as defined by $\delta^{13}C$. (a)** Scatter plot illustrating the positive
702 relationship (*P*-value < 0.05) between leaf area homeostasis in response to drought (leaf area
703 plasticity index, y-axis) and water use efficiency (x-axis) among Iberian Arabidopsis accessions used
704 in this study. Data were fitted to a linear regression model. Grey shadow represents the 95% CI of
705 the fit regression line (black). $\delta^{13}C$ data for the accessions were retrieved from Dittberner *et al.* (2018).
706 Four different quadrants are defined by two dashed lines: y = 0, which is the homeostatic point at
707 which a change in water availability does not affect relative leaf area (i.e., a plasticity index of 0),
708 and the average intrinsic water use efficiency (WUE_i, $\delta^{13}C$; x-axis). Data points depict individual
709 accessions with their respective labels. **(b)** The genetic basis of leaf area plasticity in response to
710 drought and water use efficiency. This plot depicts the respective relationship between the GWAS
711 associations found for the leaf area plasticity index in response to drought (y-axis) and those for WUE_i
712 (Dittberner *et al.*, 2018) (x-axis). Data points represent individual SNPs. The y-axis and x-axis depict
713 the extent of the association with, respectively, leaf area plasticity, and WUE_i, as the negative
714 logarithm of the p-value. Dashed lines depict an arbitrary threshold for significance that is consistent
715 across comparisons. **(c)** Transcriptomic association with plastic leaf area responses to drought and
716 WUE_i. Spearman's rank correlation depicts the relationship between the association of the transcript
717 abundance of each gene in the Arabidopsis genome with leaf area plasticity in response to drought
718 (r_s) on the y-axis and with WUE_i on the x-axis. Dashed lines define an arbitrary threshold to consider
719 transcripts correlated positively ($r_s \geq 0.4$) or negatively ($r_s \leq -0.4$) associated with leaf area plasticity
720 (y-axis) or WUE_i (x-axis). *CBF5* and *CNGC16* exemplify transcripts with opposing relationships to

721 leaf area plasticity and water use efficiency as shown in 4c. **d** and **e**. Scatter plots depicting the
722 relationship (P-value < 0.05) between leaf area plasticity index in response to drought (**4d**), or water
723 use efficiency (**4e**) on the y-axis, and transcript abundance (FPKM) of *CBF5* on the x-axis. **f** and **g**.
724 Scatter plots depicting the relationship (*P*-value < 0.05) between (**4f**) leaf area plasticity index in
725 response to drought or (**4g**) water use efficiency (Dittberner *et al.*, 2018) on the y-axis, and transcript
726 abundance (FPKM) of *CYCLIC NUCLEOTIDE-GATED CHANNEL 16* (*CNGC16*) on the x-axis. In
727 all panels, data were fitted using a linear regression model. Grey shadow represents the 95% CI of
728 the fit regression line.

729

730 **Figure 5. Photosynthesis-related transcript variants regulate water use efficiency in Iberian**
731 **Arabidopsis accessions. (a)** Manhattan plot representing the genome-wide strength of association
732 between genetic variation and variation in $\delta^{13}C$ present within 95 Iberian accessions with $\delta^{13}C$ values
733 available from (Dittberner *et al.*, 2018). The score (y-axis) consists of the negative logarithm of the
734 *P*-value and provides association strength. **Inset:** Violin plots representing the probability densities
735 of WUE_i for the major and minor allele haplotypes in *ClpX* for the accessions included in 5a. **(b)** T-
736 Manhattan plot representing transcriptome-wide strength of association between variation in
737 transcript abundance (Kawakatsu *et al.*, 2016) and natural variation in $\delta^{13}C$. This analysis was
738 performed on all Iberian accessions with both transcript abundance data (Kawakatsu *et al.*, 2016) and
739 $\delta^{13}C$ information (Dittberner *et al.*, 2018) (n = 88 accessions). The relationship is defined by the
740 Spearman's rank correlation coefficient (r_s). Dashed lines define an arbitrary threshold for positive
741 ($r_s \geq 0.4$) or negative ($r_s \leq -0.4$) correlation with water-use efficiency (y-axis). Blue labels highlight
742 the transcripts positively associated with higher WUE_i, while red labels highlight those negatively
743 associated with higher WUE_i. **(c)** Hierarchical clustering tree summarizing the correlation among
744 significant GO Biological Process categories resulting from analysis of the positively correlated
745 candidates resulting from TWA analysis of water use efficiency determined from δ13C values in 88
746 Iberian Arabidopsis accessions. Ratios provide the number of genes positively correlated with WUE_i
747 within each GO category relative to the total number of genes within that category. The size of the
748 blue dots increases proportionally with P-value significance. **(d)** Scatter plot depicting the positive
749 relationship (*P*-value < 0.05) between WUE_i (y-axis) and *RuBisCO SMALL SUBUNIT 2B*
750 (*AT5G38420*; *RBCS2B*) transcript abundance (x-axis) for the Iberian accessions included in 6b. **(e)**
751 Scatter plot depicting the positive relationship (*P*-value < 0.05) between intrinsic water-use efficiency

752 (WUE$_i$; y-axis) and *SMALL AUXIN UP RNA 26* (*SAUR26,* AT3G03850) transcript abundance (x-
753 axis) for the Iberian accessions included in 6b. **Inset:** Scatter plot depicting the positive relationship
754 (*P*-value < 0.05) between intrinsic water-use efficiency (WUE$_i$; y-axis) and *SMALL AUXIN UP RNA*
755 *26* (*SAUR26,* AT3G03850) transcript abundance (x-axis) for the 43 accessions included in our study.
756 For **d)**, and **e)**, gray shadow represents the 95% CI of the fit regression line (black).
757

758 **Acknowledgements**

759 This research was supported by funding from The Pennsylvania State University to S.M.A. We thank
760 Mr. Leland Burghard, Ms. Sarah Cronk, and Dr. Yotam Zait for greenhouse assistance. We thank
761 Drs. David Chakravorty and Yotam Zait for helpful comments on the manuscript.

762

763 **Author contributions**

764 S.M.A & A.F-S. conceived the project, research plans and experimental design. A.F-S. performed
765 the experiments while S.M.A provided guidance throughout the experimental work. A.F-S. analyzed
766 the data and prepared the figures; S.M.A provided supervision with data analysis and figure
767 preparation. S.M.A & A.F-S wrote the manuscript. A.F-S agrees to serve as the author responsible
768 for contact and ensuring communication and assistance with the reproducibility of the results of this
769 study.

770

771 **Data Availability**

772 The data supporting the results are available as Supporting Information files. The code and data to
773 easily reproduce the analysis, figures, and tables in this manuscript are available at
774 https://github.com/AssmannLab and will be uploaded to Zenodo upon acceptance.

775 **References**

776

777 **Abudayyeh OO, Gootenberg JS, Essletzbichler P, Han S, Joung J, Belanto JJ, Verdine V, Cox**
778 **DBT, Kellner MJ, Regev A, *et al.* 2017.** RNA targeting with CRISPR-Cas13. *Nature* **550:**
779 280–284.

Angert AL, Huxman TE, Chesson P, Venable DL. 2009. Functional tradeoffs determine species coexistence via the storage effect. *Proceedings of the National Academy of Sciences, U.S.A.* **106:** 11641–11645.

Billings WD, Mooney HA. 1968. The ecology of arctic and alpine plants. *Biological Reviews* **43:** 481–529

Bradshaw AD. 1965. Evolutionary significance of phenotypic plasticity in plants. *Elsevier*, pp 115–155.

Chapin, FS. 1991. Integrated responses of plants to stress. *Bioscience* **41:** 29–36.

Chen I-C, Hill JK, Ohlemüller R, Roy DB, Thomas CD. 2011. Rapid range shifts of species associated with high levels of climate warming. *Science* **333:** 1024–1026.

Cheng, CY, Krishnakumar, V, Chan, AP, Thibaud-Nissen, F, Schobel, S, & Town, CD. 2017. Araport11: a complete reannotation of the *Arabidopsis thaliana* reference genome. *The Plant Journal*, ***89*:** 789-804.

Cingolani P, Platts A, Wang LL, Coon M, Nguyen T, Wang L, Land SJ, Lu X, Ruden DM. 2012. A program for annotating and predicting the effects of single nucleotide polymorphisms, SnpEff: SNPs in the genome of *Drosophila melanogaster* strain w1118; iso-2; iso-3. *Fly (Austin).* **6:** 80–92.

Coll JR, Aguilar E, Ashcroft L. 2016. Drought variability and change across the Iberian Peninsula. *Theoretical and Applied Climatology* **130:** 901-916.

Condon AG, Richards RA, Rebetzke GJ, Farquhar GD. 2002. Improving intrinsic water-use efficiency and crop yield. *Crop Science* **42:** 122–131.

DeFalco TA, Moeder W, Yoshioka K. 2016. Opening the gates: insights into cyclic nucleotide-gated channel-mediated signaling. *Trends in Plant Science* **21:** 903–906.

Des Marais DL, McKay JK, Richards JH, Sen S, Wayne T, Juenger TE. 2012. Physiological genomics of response to soil drying in diverse Arabidopsis accessions. *Plant Cell* **24:** 893–914.

Dittberner H, Korte A, Mettler-Altmann T, Weber APM, Monroe G, de Meaux J. 2018. Natural variation in stomata size contributes to the local adaptation of water-use efficiency in *Arabidopsis thaliana*. *Molecular Ecology* **27:** 4052–4065.

Donat MG, Lowry AL, Alexander LV, O'Gorman PA, Maher N. 2016. More extreme precipitation in the world's dry and wet regions. *Nature Climate Change* **6:** 508–513.

Dorn LA, Pyle EH, Schmitt J. 2000. Plasticity to light cues and resources in *Arabidopsis thaliana*: testing for adaptive value and costs. *Evolution* **54:** 1982–1994.

Easlon HM, Nemali KS, Richards JH, Hanson DT, Juenger TE, McKay JK. 2014. The physiological basis for genetic variation in water use efficiency and carbon isotope composition in *Arabidopsis thaliana*. *Photosynthesis Research* **119:** 119–129.

Easterling DR, Meehl GA, Parmesan C, Changnon SA, Karl TR, Mearns LO. 2000. Climate extremes: observations, modeling, and impacts. *Science* **289:** 2068–2074.

Emenecker, R. J., & Strader, L. C. 2020. Auxin-abscisic acid interactions in plant growth and development. *Biomolecules*, **10:** 281.

Exposito-Alonso M, 500 Genomes Field Experiment Team, Burbano HA, Bossdorf O, Nielsen R, Weigel D. 2019. Natural selection on the *Arabidopsis thaliana* genome in present and future climates. *Nature* **573:** 126–129.

Exposito-Alonso M, Brennan AC, Alonso-Blanco C, Picó FX. 2018a. Spatio-temporal variation in fitness responses to contrasting environments in *Arabidopsis thaliana*. *Evolution* **72:** 1570-1586.

Exposito-Alonso M, Vasseur F, Ding W, Wang G, Burbano HA, Weigel D. 2018b. Genomic basis and evolutionary potential for extreme drought adaptation in *Arabidopsis thaliana*. *Nature Ecology & Evolution* **2:** 352–358.

Ferguson JN, Fernandes SB, Monier B, Miller ND, Allan D, Dmitrieva A, Schmuker P, Lozano R, Valluru R, Buckler ES, et al. 2020. Machine learning enabled phenotyping for GWAS and TWAS of WUE traits in 869 field-grown sorghum accessions. *Plant Physiology* 10.1093/plphys/kiab346.

Ferrero-Serrano Á, Assmann SM. 2019. Phenotypic and genome-wide association with the local environment of Arabidopsis. *Nature Ecology & Evolution* **3:** 274–285.

Ferrero-Serrano Á, Assmann SM. 2016. The α-subunit of the rice heterotrimeric G protein, RGA1, regulates drought tolerance during the vegetative phase in the dwarf rice mutant *d1*. *Journal of Experimental Botany* **67:** 3433–3443.

Ferrero-Serrano Á, Su Z, Assmann SM. 2018. Illuminating the role of the Gα heterotrimeric G protein subunit, *RGA1*, in regulating photoprotection and photoavoidance in rice. *Plant, Cell & Environment* **41:** 451–468.

Forsman A. 2015. Rethinking phenotypic plasticity and its consequences for individuals, populations

842 and species. *Heredity* **115:** 276–284.
843 **Frachon L, Bartoli C, Carrère S, Bouchez O, Chaubet A, Gautier M, Roby D, Roux F. 2018.** A
844 genomic map of climate adaptation in *Arabidopsis thaliana* at a micro-geographic scale.
845 *Frontiers in Plant Sciences* **9:** 967.
846 **Frachon L, Mayjonade B, Bartoli C, Hautekèete N-C, Roux F. 2019.** Adaptation to plant
847 communities across the genome of *Arabidopsis thaliana*. Molecular Biology & Evolution **36:**
848 1442–1456.
849 F**reudenthal, JA, Ankenbrand, MJ, Grimm, DG, & Korte, A. 2019.** GWAS-Flow: A GPU
850 accelerated framework for efficient permutation based genome-wide association studies.
851 *BioRxiv.* doi: 10.1101/783100.
852 **Ge SX, Jung D, Yao R. 2020.** ShinyGO: a graphical gene-set enrichment tool for animals and plants.
853 *Bioinformatics* **36:** 2628–2629.
854 **Ghalambor CK, McKAY JK, Carroll SP, Reznick DN. 2007.** Adaptive versus non-adaptive
855 phenotypic plasticity and the potential for contemporary adaptation in new environments.
856 *Functional Ecology* **21:** 394–407.
857 **Gomaa NH, Montesinos-Navarro A, Alonso-Blanco C, Picó FX. 2011.** Temporal variation in
858 genetic diversity and effective population size of Mediterranean and subalpine *Arabidopsis*
859 *thaliana* populations. *Molecular Ecology* **20:** 3540–3554.
860 **Grime JP. 1977.** Evidence for the existence of three primary strategies in plants and its relevance to
861 ecological and evolutionary theory. *The American Naturalist* **111:** 1169–1194.
862 **Groszmann M, Osborn HL, Evans JR. 2017.** Carbon dioxide and water transport through plant
863 aquaporins. *Plant, Cell & Environment* **40:** 938–961.
864 **Gusev A, Ko A, Shi H, Bhatia G, Chung W, Penninx BWJH, Jansen R, de Geus EJC, Boomsma**
865 **DI, Wright FA, et al. 2016.** Integrative approaches for large-scale transcriptome-wide
866 association studies. *Nature Genetics* **48:** 245–252.
867 **Haldrup A, Naver H, Scheller HV. 1999.** The interaction between plastocyanin and photosystem I
868 is inefficient in transgenic Arabidopsis plants lacking the *PSI-N* subunit of photosystem I. *The*
869 *Plant Journal* **17:** 689–698.
870 **Harrell Jr F, Dupont C. 2019.** Package 'Hmisc'. CRAN2018 2019: 235–6.
871 **Heinsch FA, Reeves M, Votava P, Kang S, Milesi C, Zhao M, Glassy J, Jolly WM, Loehman R,**
872 **Bowker CF, *et al*. 2003.** Gpp and npp (mod17a2/a3) products nasa modis land algorithm.

873 MOD17 User's Guide 1–57.
874 **Holt RD. 1990.** The microevolutionary consequences of climate change. *Trends in Ecology &*
875 *Evolution* **5:** 311–315.
876 **Huang, L, He, B, Chen, A, Wang, H, Liu, J, Lű, A, & Chen, Z. 2016.** Drought dominates the
877 interannual variability in global terrestrial net primary production by controlling semi-arid
878 ecosystems. *Scientific reports* ***6*****:** 1-7.
879 **Ifuku K, Endo T, Shikanai T, Aro E-M. 2011.** Structure of the chloroplast NADH dehydrogenase-
880 like complex: nomenclature for nuclear-encoded subunits. *Plant & Cell Physiology* **52:** 1560–
881 1568.
882 **IRRI. 2021.** Phenotyping protocols for abiotic stress tolerance in rice. International Rice Research
883 Institute, Los Baños, Phillipines.
884 **Juenger TE, McKay JK, Simms EI, Richards JH. 2005.** Identification and characterization of QTL
885 underlying whole-plant physiology in *Arabidopsis thaliana*: $\delta^{13}C$, stomatal conductance and
886 transpiration efficiency. *Plant, Cell & Environment* **28:** 697–708.
887 **Karijolich, J., Yi, C., & Yu, Y. T. 2015.** Transcriptome-wide dynamics of RNA
888 pseudouridylation. *Nature reviews Molecular cell biology*, **16:** 581-585.
889 **Kasuga M, Liu Q, Miura S, Yamaguchi-Shinozaki K, Shinozaki K . 1999.** Improving plant
890 drought, salt, and freezing tolerance by gene transfer of a single stress-inducible transcription
891 factor. *Nature Biotechnology* **17:** 287–291.
892 **Kawakatsu T, Huang S-SC, Jupe F, Sasaki E, Schmitz RJ, Urich MA, Castanon R, Nery JR,**
893 **Barragan C, He Y, *et al*. 2016.** Epigenomic diversity in a global collection of *Arabidopsis*
894 *thaliana* accessions. *Cell* **166:** 492–505.
895 **Kim J, Rudella A, Ramirez Rodriguez V, Zybailov B, Olinares PDB, van Wijk KJ. 2009.**
896 Subunits of the plastid ClpPR protease complex have differential contributions to
897 embryogenesis, plastid biogenesis, and plant development in Arabidopsis. *The Plant Cell* **21:**
898 1669–1692.
899 **Kimball S, Gremer JR, Angert AL, Huxman TE, Venable DL . 2012.** Fitness and physiology in
900 a variable environment. *Oecologia 169:* 319–329.
901 **van Kleunen M, Fischer M. 2005.** Constraints on the evolution of adaptive phenotypic plasticity in
902 plants. *New Phytologist* **166:** 49–60.
903 **Köhler C, Merkle T, Neuhaus G. 1999.** Characterisation of a novel gene family of putative cyclic

904 nucleotide- and calmodulin-regulated ion channels in *Arabidopsis thaliana*. *The Plant Journal*
905 **18:** 97–104.
906 **Korte A, Farlow A. 2013.** The advantages and limitations of trait analysis with GWAS: a review.
907 *Plant Methods* **9:** 29.
908 **Kramer, M. C., Janssen, K. A., Palos, K., Nelson, A. D., Vandivier, L. E., Garcia, B. A., ... &**
909 **Gregory, B. D. 2020.** N6-methyladenosine and RNA secondary structure affect transcript
910 stability and protein abundance during systemic salt stress in Arabidopsis. e00239
911 **Kremling KAG, Diepenbrock CH, Gore MA, Buckler ES, Bandillo NB. 2019.** Transcriptome-
912 wide association supplements genome-wide association in *Zea mays*. *G3: Genes, Genomes,*
913 *Genetics* **9:** 3023–3033.
914 **Lasky JR, Des Marais DL, Lowry DB, Povolotskaya I, McKay JK, Richards JH, Keitt TH,**
915 **Juenger TE. 2014.** Natural variation in abiotic stress responsive gene expression and local
916 adaptation to climate in *Arabidopsis thaliana*. Molecular Biology and Evolution **31:** 2283–
917 2296.
918 **Lermontova, I., Schubert, V., Börnke, F., Macas, J., & Schubert, I. 2007.** Arabidopsis CBF5
919 interacts with the H/ACA snoRNP assembly factor NAF1. *Plant molecular biology* ***65*:** 615-
920 626.
921 **Leyser HM, Pickett FB, Dharmasiri S, Estelle M. 1996.** Mutations in the *AXR3* gene of
922 Arabidopsis result in altered auxin response including ectopic expression from the *SAUR-AC1*
923 promoter. *The Plant Journal* **10:** 403–413.
924 **Li Z-G, Chen H-W, Li Q-T, Tao J-J, Bian X-H, Ma B, Zhang W-K, Chen S-Y, Zhang J-S. 2015.**
925 Three SAUR proteins *SAUR76*, *SAUR77* and *SAUR78* promote plant growth in Arabidopsis.
926 *Scientific Reports* **5:** 12477.
927 Li, D., Liu, Q., & Schnable, P. S. (2021). TWAS results are complementary to and less affected by
928 linkage disequilibrium than GWAS. *Plant Physiology* 186: 1800-1811.
929 **Livingston AK, Cruz JA, Kohzuma K, Dhingra A, Kramer DM. 2010.** An Arabidopsis mutant
930 with high cyclic electron flow around photosystem I . hcef. involving the NADPH
931 dehydrogenase complex. *Plant Cell* **22:** 221–233.
932 **Lobo JM, Castro I, Moreno JC. 2001.** Spatial and environmental determinants of vascular plant
933 species richness distribution in the Iberian Peninsula and Balearic Islands. *Biological Journal*
934 *of the Linnean Society* **73:** 233–253.

935 **Maiwald D, Dietzmann A, Jahns P, Pesaresi P, Joliot P, Joliot A, Levin JZ, Salamini F, Leister**
936 **D. 2003.** Knock-out of the genes coding for the Rieske protein and the ATP-synthase delta-
937 subunit of Arabidopsis. Effects on photosynthesis, thylakoid protein composition, and nuclear
938 chloroplast gene expression. *Plant Physiology* **133:** 191–202.
939 **Manzano-Piedras E, Marcer A, Alonso-Blanco C, Picó FX. 2014.** Deciphering the adjustment
940 between environment and life history in annuals: lessons from a geographically-explicit
941 approach in *Arabidopsis thaliana*. *PLoS One* **9:** e87836.
942 **Marcer A, Vidigal DS, James PMA, Fortin MJ, Méndez-Vigo B, Hilhorst HWM, Bentsink L,**
943 **Alonso-Blanco C, Picó FX. 2018.** Temperature fine-tunes Mediterranean *Arabidopsis*
944 *thaliana* life-cycle phenology geographically. Plant Biology **20:** 148–156.
945 **Meehl GA, Tebaldi C. 2004.** More intense, more frequent, and longer lasting heat waves in the 21st
946 century. *Science* **305:** 994–997.
947 **Méndez-Vigo B, Picó FX, Ramiro M, Martínez-Zapater JM, Alonso-Blanco C. 2011.** Altitudinal
948 and climatic adaptation is mediated by flowering traits and FRI, FLC, and PHYC genes in
949 Arabidopsis. *Plant Physiology* **157:** 1942–1955.
950 **Montesinos A, Tonsor SJ, Alonso-Blanco C, Picó FX. 2009.** Demographic and genetic patterns of
951 variation among populations of *Arabidopsis thaliana* from contrasting native environments.
952 *PLoS One* **4:** e7213.
953 **Montesinos-Navarro A, Wig J, Pico FX, Tonsor SJ. 2011.** *Arabidopsis thaliana* populations show
954 clinal variation in a climatic gradient associated with altitude. *New Phytologist* **189:** 282–294.
955 **Murakami R, Ifuku K, Takabayashi A, Shikanai T, Endo T, Sato F. 2005.** Functional dissection
956 of two Arabidopsis PsbO proteins: *PsbO1* and *PsbO2*. *The FEBS Journal* **272**: 2165–2175.
957 **Nagatoshi Y, Ikeda M, Kishi H, Hiratsu K, Muraguchi A, Ohme-Takagi M. 2016.** Induction of
958 a dwarf phenotype with IBH1 may enable increased production of plant-made
959 pharmaceuticals in plant factory conditions. *Plant Biotechnology Journal* **14:** 887–894.
960 **Nilson, S. E., & Assmann, S. M. 2010.** Heterotrimeric G proteins regulate reproductive trait
961 plasticity in response to water availability. *New Phytologist*, **185***:* 734-746.
962 **Nishimura K, van Wijk KJ . 2015.** Organization, function and substrates of the essential Clp
963 protease system in plastids. *Biochimica et Biophysica Acta* **1847:** 915–930.
964 **Oh E, Zhu J-Y, Bai M-Y, Arenhart RA, Sun Y, Wang Z-Y. 2014.** Cell elongation is regulated
965 through a central circuit of interacting transcription factors in the Arabidopsis hypocotyl.

966 *Elife*. doi: 10.7554/eLife.03031.
967 **Ohashi-Ito K, Matsukawa M, Fukuda H. 2013.** An atypical bHLH transcription factor regulates
968 early xylem development downstream of auxin. Plant Cell Physiol **54:** 398–405.
969 **Parsons RF. 1968.** The significance of growth-rate comparisons for plant ecology. The American
970 Naturalist **102:** 595–597.
971 **Páscoa P, Gouveia CM, Russo A, Trigo RM. 2017.** Drought Trends in the Iberian Peninsula over
972 the Last 112 Years. *Advances in Meteorology* **2017:** 1–13.
973 **Picó FX. 2012.** Demographic fate of *Arabidopsis thaliana* cohorts of autumn- and spring-germinated
974 plants along an altitudinal gradient. *Journal of Ecology* **100:** 1009–1018.
975 **Picó FX, Méndez-Vigo B, Martínez-Zapater JM, Alonso-Blanco C. 2008.** Natural genetic
976 variation of *Arabidopsis thaliana* is geographically structured in the Iberian peninsula.
977 *Genetics* **180:** 1009–1021.
978 **Price AL, Zaitlen NA, Reich D, Patterson N. 2010.** New approaches to population stratification in
979 genome-wide association studies. Nature Reviews Genetics **11:** 459–463.
980 **Rey Benayas JM, Scheiner SM. 2002.** Plant diversity, biogeography and environment in Iberia:
981 Patterns and possible causal factors. *Journal of Vegetation Science* **13:** 245.
982 **Running SW, Zhao M. 2015.** Daily GPP and annual NPP . MOD17A2/A3. products NASA Earth
983 Observing System MODIS land algorithm. MOD17 User's Guide 2015: 1–28.
984 **Salehin M, Li B, Tang M, Katz E, Song L, Ecker JR, Kliebenstein DJ, Estelle M. 2019.** Auxin-
985 sensitive Aux/IAA proteins mediate drought tolerance in Arabidopsis by regulating
986 glucosinolate levels. *Nature Communications* **10:** 4021.
987 **Schär C, Vidale PL, Lüthi D, Frei C, Häberli C, Liniger MA, Appenzeller C. 2004.** The role of
988 increasing temperature variability in European summer heatwaves. *Nature* **427:** 332–336
989 **Schindele A, Dorn A, Puchta H. 2020.** CRISPR/Cas brings plant biology and breeding into the fast
990 lane. *Current Opinion in Biotechnology* **61:** 7–14.
991 **Schweizer F, Fernández-Calvo P, Zander M, Diez-Diaz M, Fonseca S, Glauser G, Lewsey MG,**
992 **Ecker JR, Solano R, Reymond P. 2013.** Arabidopsis basic helix-loop-helix transcription
993 factors MYC2, MYC3, and MYC4 regulate glucosinolate biosynthesis, insect performance,
994 and feeding behavior. *Plant Cell* **25:** 3117–3132.
995 **Seren Ü, Vilhjálmsson BJ, Horton MW, Meng D, Forai P, Huang YS, Long Q, Segura V,**
996 **Nordborg M. 2012.** GWAPP: a web application for genome-wide association mapping in

997 Arabidopsis. *Plant Cell* **24:** 4793–4805.
998 **Siepielski AM, Morrissey MB, Buoro M, Carlson SM, Caruso CM, Clegg SM, Coulson T,**
999 **DiBattista J, Gotanda KM, Francis CD, *et al*. 2017.** Precipitation drives global variation in
1000 natural selection. *Science* **355:** 959–962.
1001 **Spartz AK, Ren H, Park MY, Grandt KN, Lee SH, Murphy AS, Sussman MR, Overvoorde PJ,**
1002 **Gray WM. 2014.** SAUR inhibition of PP2C-D Phosphatases activates plasma membrane H^+-
1003 ATPases to promote cell expansion in Arabidopsis. *Plant Cell* **26:** 2129–2142
1004 **Stortenbeker N, Bemer M. 2019.** The SAUR gene family: the plant's toolbox for adaptation of
1005 growth and development. *Journal of Experimental Botany* **70:** 17–27.
1006 T**abas-Madrid D, Méndez-Vigo B, Arteaga N, Marcer A, Pascual-Montano A, Weigel D, Xavier**
1007 **Picó F, Alonso-Blanco C. 2018.** Genome-wide signatures of flowering adaptation to climate
1008 temperature: regional analyses in a highly diverse native range of *Arabidopsis thaliana*. *Plant,*
1009 *Cell & Environment* **41:** 1806–1820.
1010 **Tang, Y., Gao, C. C., Gao, Y., Yang, Y., Shi, B., Yu, J. L., ... & Chong, K. (2020).** OsNSUN2-
1011 mediated 5-methylcytosine mRNA modification enhances rice adaptation to high
1012 temperature. *Developmental cell* ***53*****:** 272-286.
1013 **Team RC . 2013.** R: A language and environment for statistical computing.
1014 **The 1001 Genomes Consortium** 2016. 1,135 Genomes reveal the global pattern of polymorphism
1015 in *Arabidopsis thaliana*. *Cell* **166:** 481–491.
1016 **Tilman D. 1988.** Plant strategies and the dynamics and structure of plant communities. Princeton
1017 University Press.
1018 **Tunc-Ozdemir M, Tang C, Ishka MR, Brown E, Groves NR, Myers CT, Rato C, Poulsen LR,**
1019 **McDowell S, Miller G, *et al*. 2013.** A cyclic nucleotide-gated channel . CNGC16. in pollen
1020 is critical for stress tolerance in pollen reproductive development. *Plant Physiology* **161:**
1021 1010–1020.
1022 **Via S, Gomulkiewicz R, De Jong G, Scheiner SM, Schlichting CD, Van Tienderen PH. 1995.**
1023 Adaptive phenotypic plasticity: consensus and controversy. *Trends in Ecology & Evolution*.
1024 **10:** 212–217.
1025 **Vicente-Serrano SM. 2006a.** Spatial and temporal analysis of droughts in the Iberian Peninsula .
1026 1910–2000. *Hydrological Sciences Journal* **51:** 83–97
1027 **Vicente-Serrano SM. 2006b.** Differences in spatial patterns of drought on different time scales: an

1028 analysis of the iberian peninsula. Water Resources Management **20:** 37–60.
1029 **Vidigal DS, Marques ACSS, Willems LAJ, Buijs G, Méndez-Vigo B, Hilhorst HWM, Bentsink**
1030 **L, Picó FX, Alonso-Blanco C. 2016.** Altitudinal and climatic associations of seed dormancy
1031 and flowering traits evidence adaptation of annual life cycle timing in *Arabidopsis thaliana*.
1032 *Plant, Cell & Environment* **39:** 1737–1748.
1033 **Wang Y-F, Munemasa S, Nishimura N, Ren H-M, Robert N, Han M, Puzõrjova I, Kollist H,**
1034 **Lee S, Mori I, *et al*. 2013.** Identification of cyclic GMP-activated nonselective Ca2+-
1035 permeable cation channels and associated CNGC5 and CNGC6 genes in Arabidopsis guard
1036 cells. *Plant Physiology* **163:** 578–590.
1037 **Wang Z, Yang L, Liu Z, Lu M, Wang M, Sun Q, Lan Y, Shi T, Wu D, Hua J. 2019.** Natural
1038 variations of growth thermo-responsiveness determined by SAUR26/27/28 proteins in
1039 *Arabidopsis thaliana*. *New Phytologist* **224:** 291–305.
1040 **Wang Z, Yang L, Wu D, Zhang N, Hua J. 2021.** Polymorphisms in cis-elements confer SAUR26
1041 gene expression difference for thermo-response natural variation in Arabidopsis. *New*
1042 *Phytologist* **229:** 2751–2764.
1043 **Weijschedé, J, Martínková, J, De Kroon, H, & Huber, H. 2006.** Shade avoidance in *Trifolium*
1044 *repens*: costs and benefits of plasticity in petiole length and leaf size. *New Phytologist* ***172:***
1045 655-666.
1046 **West-Eberhard MJ. 2003.** Developmental plasticity and evolution. Oxford University Press
1047 **Wickham H, Francois R, Henry L, Müller K. 2015.** dplyr: A grammar of data manipulation. R
1048 package version 0.4 3.
1049 **Wickham H, Henry L. 2018.** tidyr: Easily Tidy Data with 'spread 'and 'gather'Functions. R package
1050 version 0.8 2.
1051 **Wolfe MD, Tonsor SJ. 2014.** Adaptation to spring heat and drought in northeastern Spanish
1052 *Arabidopsis thaliana*. *New Phytologist* **201:** 323–334.
1053 **Wong, J. H., Klejchová, M., Snipes, S. A., Nagpal, P., Bak, G., Wang, B., ... & Gray, W. M.**
1054 **2021.** SAUR proteins and PP2C. D phosphatases regulate H^+-ATPases and K+ channels to
1055 control stomatal movements. *Plant physiology* **185:** 256-273.
1056 **Yamori W, Sakata N, Suzuki Y, Shikanai T, Makino A. 2011.** Cyclic electron flow around
1057 photosystem I via chloroplast NAD. P.H dehydrogenase. NDH. complex performs a
1058 significant physiological role during photosynthesis and plant growth at low temperature in

1059 rice. *Plant Journal* **68:** 966–976.
1060 **Zhang H, Zhao Y, Zhu J-K. 2020.** Thriving under stress: how plants balance growth and the stress
1061 response. *Developmental Cell* **55:** 529–543.
1062 **Zheng Q, Zheng Y, Ji H, Burnie W, Perry SE. 2016.** Gene regulation by the *AGL15* transcription
1063 factor reveals hormone interactions in somatic embryogenesis. *Plant Physiology* **172:** 2374–
1064 2387.
1065

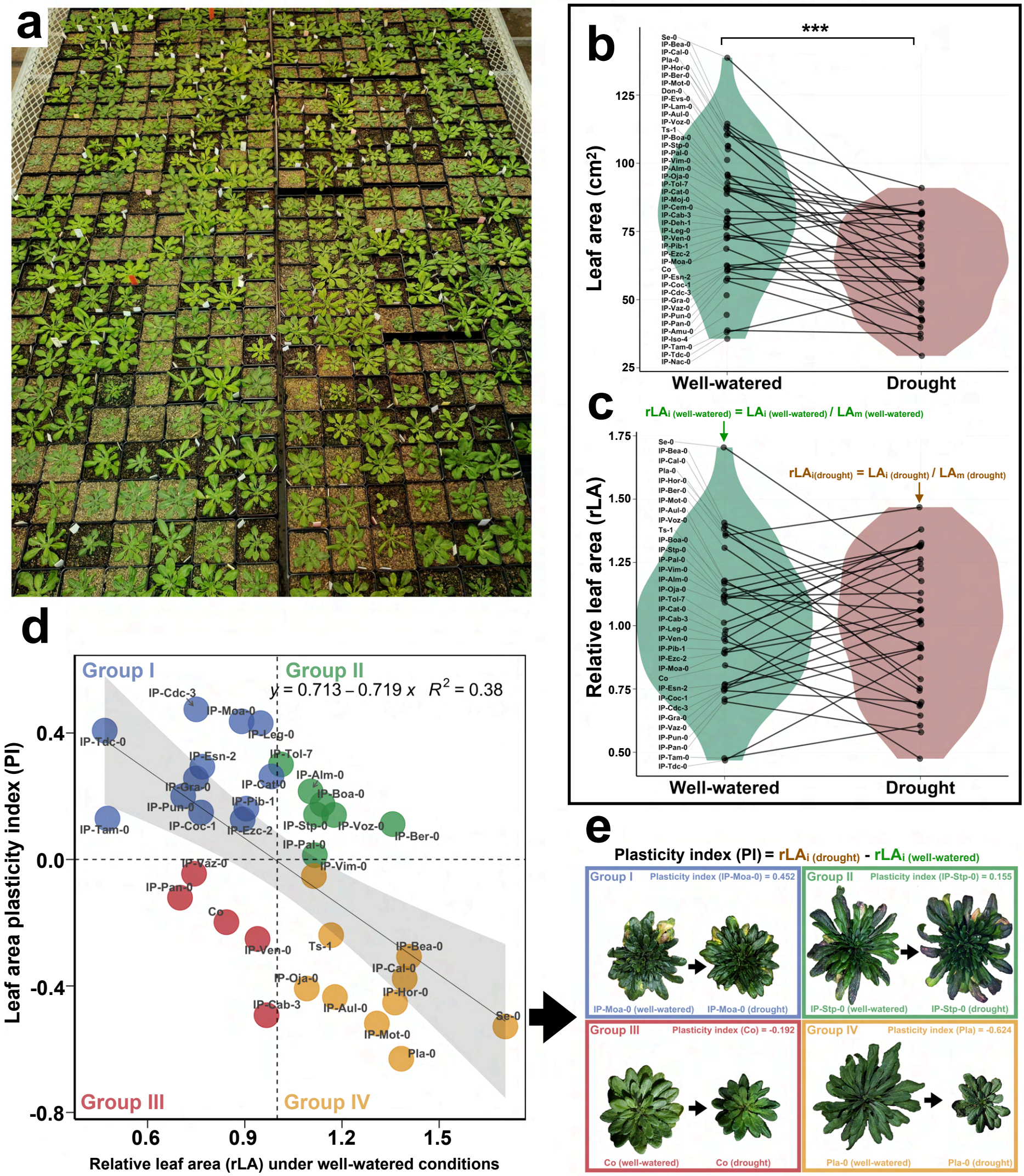

Figure 1. Arabidopsis rosette leaf area observations. **(a)** Detail of the common garden experiment, illustrating the randomization of well-watered and drought treatments, as reflected in soil coloration. **(b)** Phenotypic reaction norms illustrating a reduction of leaf area in response to drought in most but not all accessions. Violin distributions represent probability densities of leaf area (cm^2) among the accessions included in this study. Datapoints depict the mean phenotypic values of individual accessions, and the reaction norms represent the plastic response in the leaf area of each accession in response to drought (t-test; P-value < 0.001). **(c)** Phenotypic reaction norms illustrating plastic and homeostatic responses in relative leaf area (rLA). Violin distributions represent probability densities of rLA among the accessions included in this study. Datapoints depict the rLA of individual accessions, and the reaction norms represent the plastic response in rLA of each accession in response to drought (t-test; P-value > 0.05). **(d)** Negative relationship (P-value < 0.05) between leaf area plasticity index (slope of the reaction norms in 1c) in response to drought (y-axis) and rLA under well-watered conditions (x-axis). Data were fitted using a linear regression model. Grey shadow represents the 95% CI of the fit regression line. Four different quadrants are defined by two dashed lines: the average rLA (x-axis), and y = 0, which is the homeostatic point at which a change in water availability does not affect rLA (i.e. a plasticity index of 0). Data points depict individual accessions with their respective label. Data points are colored based on in which quadrant they fall (see text). **(e)** Images illustrating the plastic and homeostatic responses to drought found among the accessions included in this study.

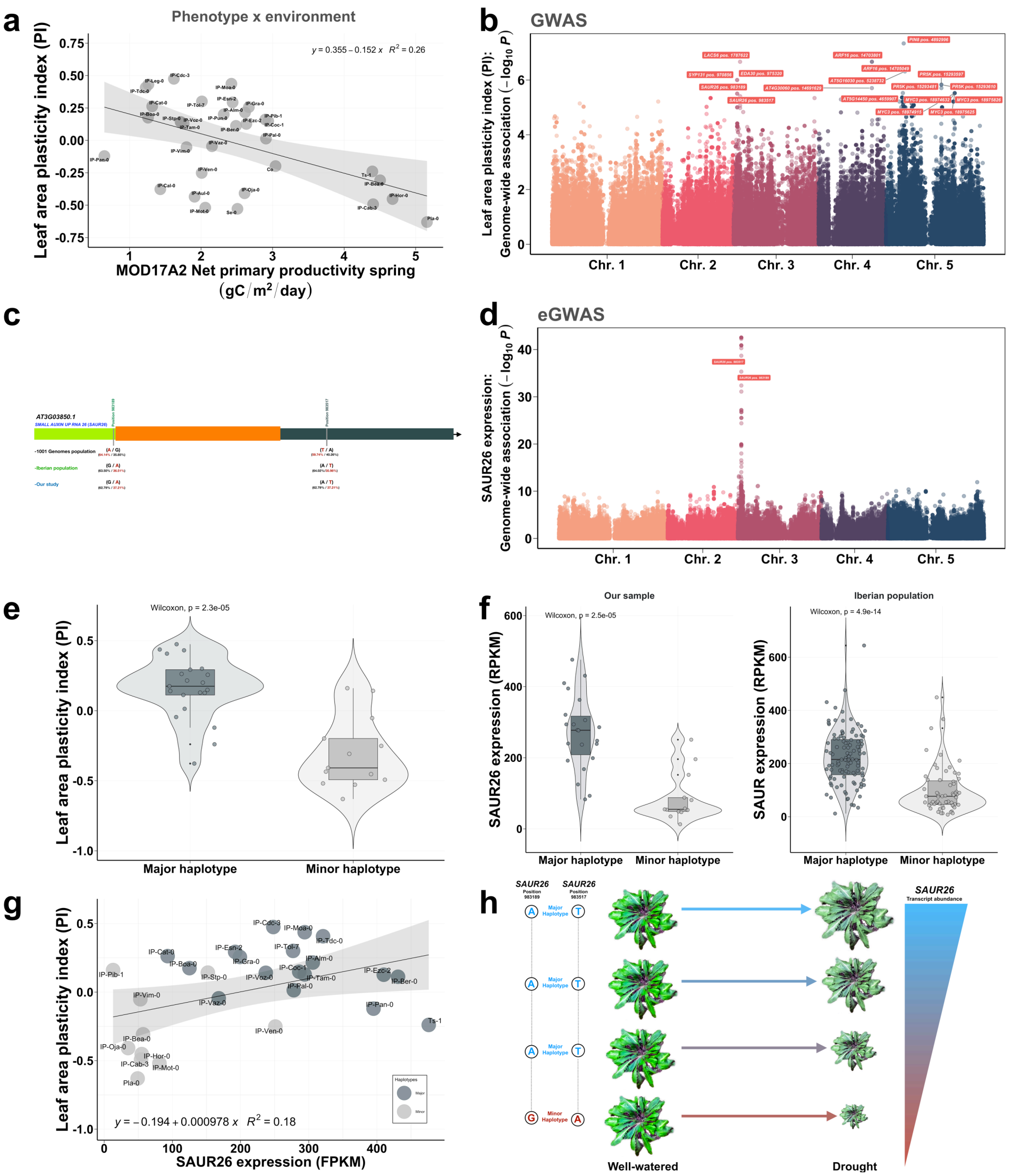

Figure 2. ***SMALL AUXIN UP RNA 26*** **(*SAUR26*, AT3G03850) is a candidate regulator of Arabidopsis leaf plasticity in response to drought. (a)** Accessions from more productive areas display stronger negative reductions in leaf area plasticity relative to accessions from less productive environments. Scatter plot depicting the negative relationship (P-value < 0.05) between leaf area plasticity index (y-axis) and Net Primary Productivity during the spring season (x-axis). **(b)** Manhattan plot representing the strength of association between genetic variants and leaf area plasticity in response to drought. **C.** *SAUR26* gene model, including the two co-varying SNPs highlighted in 2b. Orange block depicts the sole exon, green block the 5' UTR, dark green block the 3' UTR. Labels above indicate the position of the two SNPs that co-vary, forming a haplotype in our sample. Major/minor allele frequency in our sample, in the 189 accessions from the Iberian Peninsula included in the 1001 Genome Project, and in the whole 1001 Genomes Project sample dataset is provided. **(d)** Manhattan plot representing the genome-wide strength of association between the genetic variation present within the 665 accessions from the transcript abundance reference panel (Kawakatsu *et al.*, 2016) that overlap with the collection of accessions included in the 1001 Genomes Project, and the variation in the transcript abundance of *SAUR26* (Kawakatsu *et al.*, 2016). The peak in chromosome 3 represents the cis-genetic variants in *SAUR26* affecting its transcript abundance. For the Manhattan plots in 2**b** and **e**, the score (y-axis) consists of the negative logarithm of the P-value and provides association strength. Each data point represents a SNP with a color corresponding to the chromosome where the genetic variants are located. The x-axis and the different colors shown in the SNPs depicted in the Manhattan plots represent the different chromosomes. The higher the score, the lower the P-value, and the stronger the association between genetic variation and leaf area plasticity or *SAUR26* transcript abundance. **(e)** The major haplotype of *SAUR26* is associated with homeostatic or positive responses of relative leaf area (rLA) in response to drought. Conversely, the minor haplotype is associated with plastic responses in rLA in response to drought. Violin plots show significantly different probability densities of leaf area plasticity in response to drought for the major and minor allele haplotypes in *SAUR26*. **(f)** The haplotypes in *SAUR26* associated with leaf area plasticity/homeostasis in response to drought are associated with difference in *SAUR26* gene expression. Violin plots show significantly different probability densities of *SAUR26* transcript abundance for the major and minor allele haplotypes in *SAUR26* for both our sample and the entire Iberian population. **(g)** Scatter plot illustrating the positive relationship between leaf area plasticity index (y-axis) and *SAUR26* transcript abundance (x-axis). For **2**a and **2g**, the grey shadow represents the 95% CI of the fit regression line (dark grey). **(h)** Cartoon illustrating the regulatory role of genetic and transcript variation in *SAUR26* and the response of leaf area to drought.

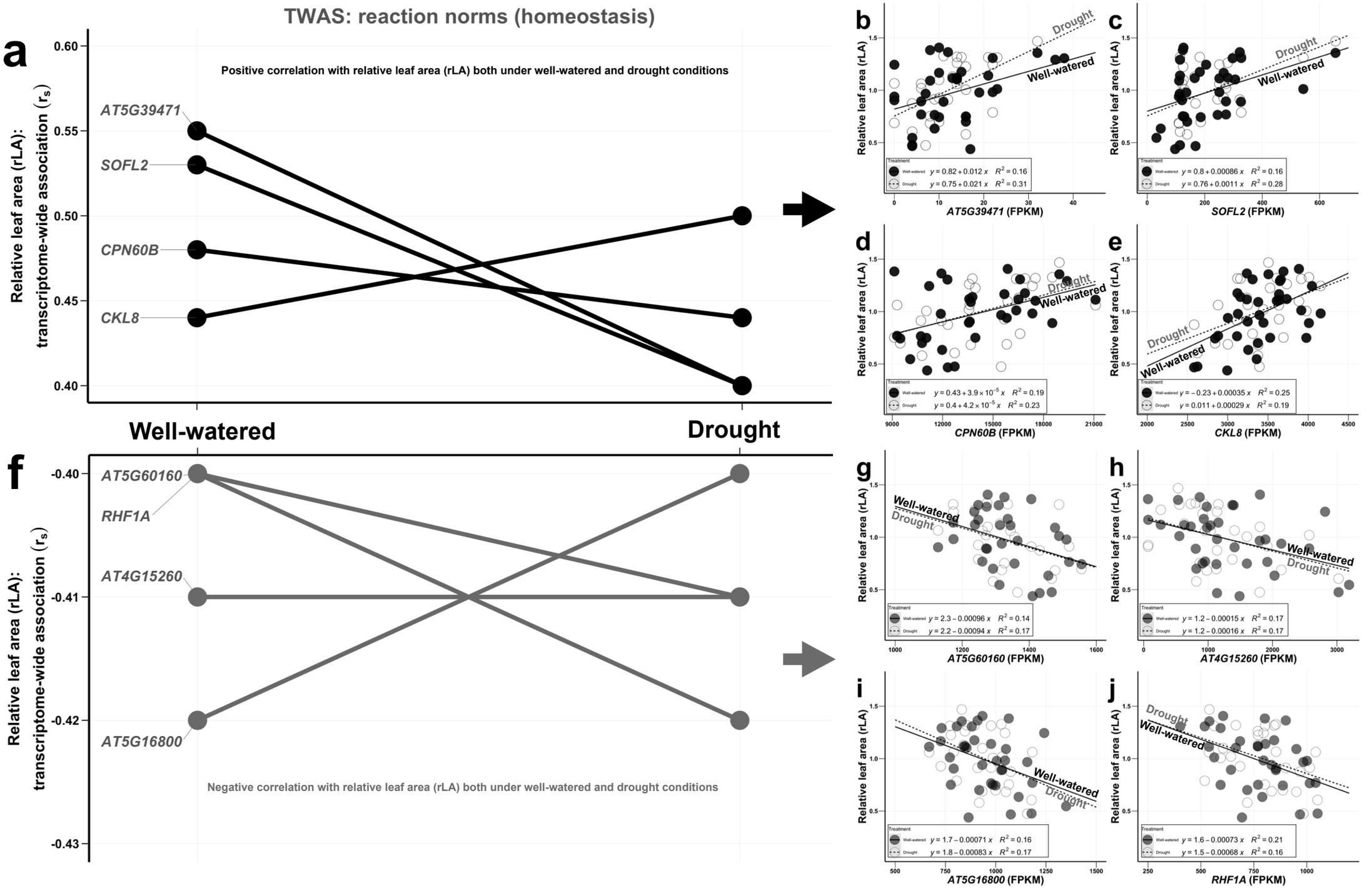

Figure 3. Transcriptomic reaction norms uncover genetic correlates of Arabidopsis leaf area homeostasis in response to drought. (a) homeostatic reaction norms for transcripts significantly and positively correlated with relative leaf area (rLA) under both watering regimes. (b) to (e). Scatter plots illustrating positive and homeostatic relationships (*P*-value < 0.05) between rLA under both well-watered (closed circles) and drought conditions (open circles) conditions (y-axis), and transcript abundance (FPKM; x-axis) of **(b)** AT5G39471, **(c)** *SOB FIVE-LIKE 2* (*SOFL2; AT1G68870*)**, (d)** *CHAPERONIN 60 BETA* (*CPN60B*; *AT1G55490*), and **(e)** *CASEIN KINASE I-LIKE 8* (*CKL8*; *AT5G43320*). **(f)** homeostatic reaction norms for transcripts significantly and negatively correlated with rLA under both watering regimes. (g) to (j) Scatter plots illustrating negative and homeostatic relationships (*P*-value < 0.05) between rLA under both well-watered (closed circles) and drought conditions (open circles) (y-axis), and transcript abundance (FPKM; x-axis) of **(g)** AT5G60160, **(h)** *AT4G15260*, **(i)** *AT5G16800*, and **(j)** *RING-H2 GROUP F1A* (*RHF1A*; *AT4G14220*). For 3a and 3f, Spearman's rank correlation coefficient ($r_{s;}$ y-axis) indicates the correlation between the rLA and the natural variation in transcript abundance of each gene. In figures b to e and g-j, data were fitted using a linear regression model. Also, in panels b-e and g-j, filled circles depict the rLA of accessions grown under well-watered conditions, while empty circles squares depict the rLA of accessions grown under drought.

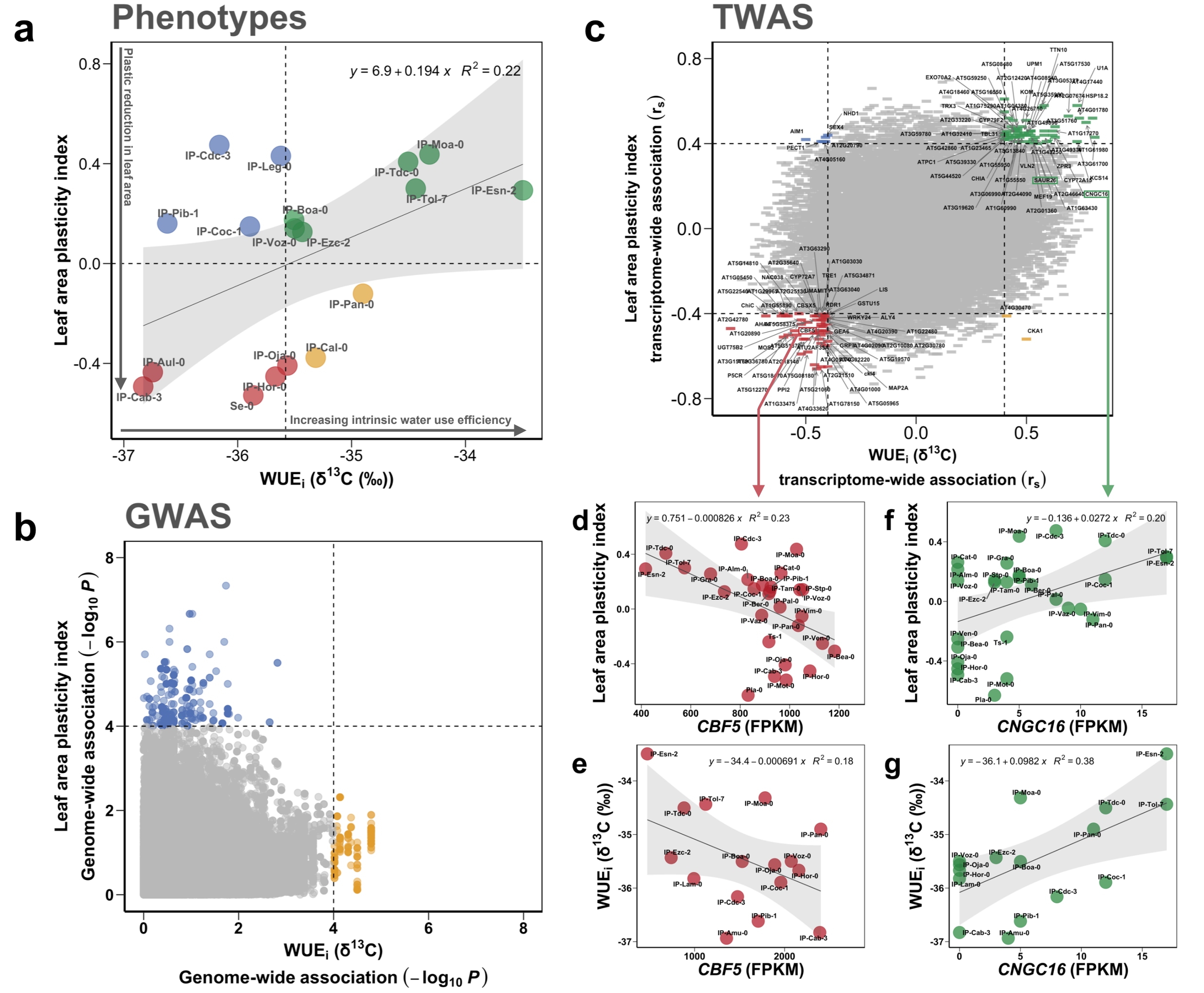

Figure 4. Arabidopsis accessions that display leaf area homeostasis in response to drought, display higher water use efficiency as defined by $\delta^{13}C$. (a) Scatter plot illustrating the positive relationship (*P*-value < 0.05) between leaf area homeostasis in response to drought (leaf area plasticity index, y-axis) and water use efficiency (x-axis) among Iberian Arabidopsis accessions used in this study. Data were fitted to a linear regression model. Grey shadow represents the 95% CI of the fit regression line (black). $\delta^{13}C$ data for the accessions were retrieved from Dittberner *et al.* (2018). Four different quadrants are defined by two dashed lines: y = 0, which is the homeostatic point at which a change in water availability does not affect relative leaf area (i.e., a plasticity index of 0), and the average intrinsic water use efficiency (WUE_i, $\delta^{13}C$; x-axis). Data points depict individual accessions with their respective labels. **(b)** The genetic basis of leaf area plasticity in response to drought and water use efficiency. This plot depicts the respective relationship between the GWAS associations found for the leaf area plasticity index in response to drought (y-axis) and those for WUE_i (Dittberner *et al.*, 2018) (x-axis). Data points represent individual SNPs. The y-axis and x-axis depict the extent of the association with, respectively, leaf area plasticity, and WUE_i, as the negative logarithm of the p-value. Dashed lines depict an arbitrary threshold for significance that is consistent across comparisons. **(c)** Transcriptomic association with plastic leaf area responses to drought and WUE_i. Spearman's rank correlation depicts the relationship between the association of the transcript abundance of each gene in the Arabidopsis genome with leaf area plasticity in response to drought (r_s) on the y-axis and with WUE_i on the x-axis. Dashed lines define an arbitrary threshold to consider transcripts correlated positively ($r_s \geq 0.4$) or negatively ($r_s \leq -0.4$) associated with leaf area plasticity (y-axis) or WUE_i (x-axis). *CBF5* and *CNGC16* exemplify transcripts with opposing relationships to leaf area plasticity and water use efficiency as shown in 4c. **d** and **e**. Scatter plots depicting the relationship (P-value < 0.05) between leaf area plasticity index in response to drought (**4d**), or water use efficiency (**4e**) on the y-axis, and transcript abundance (FPKM) of *CBF5* on the x-axis. **f** and **g**. Scatter plots depicting the relationship (*P*-value < 0.05) between (**4f**) leaf area plasticity index in response to drought or (**4g**) water use efficiency (Dittberner *et al.*, 2018) on the y-axis, and transcript abundance (FPKM) of *CYCLIC NUCLEOTIDE-GATED CHANNEL 16* (*CNGC16*) on the x-axis. In all panels, data were fitted using a linear regression model. Grey shadow represents the 95% CI of the fit regression line.

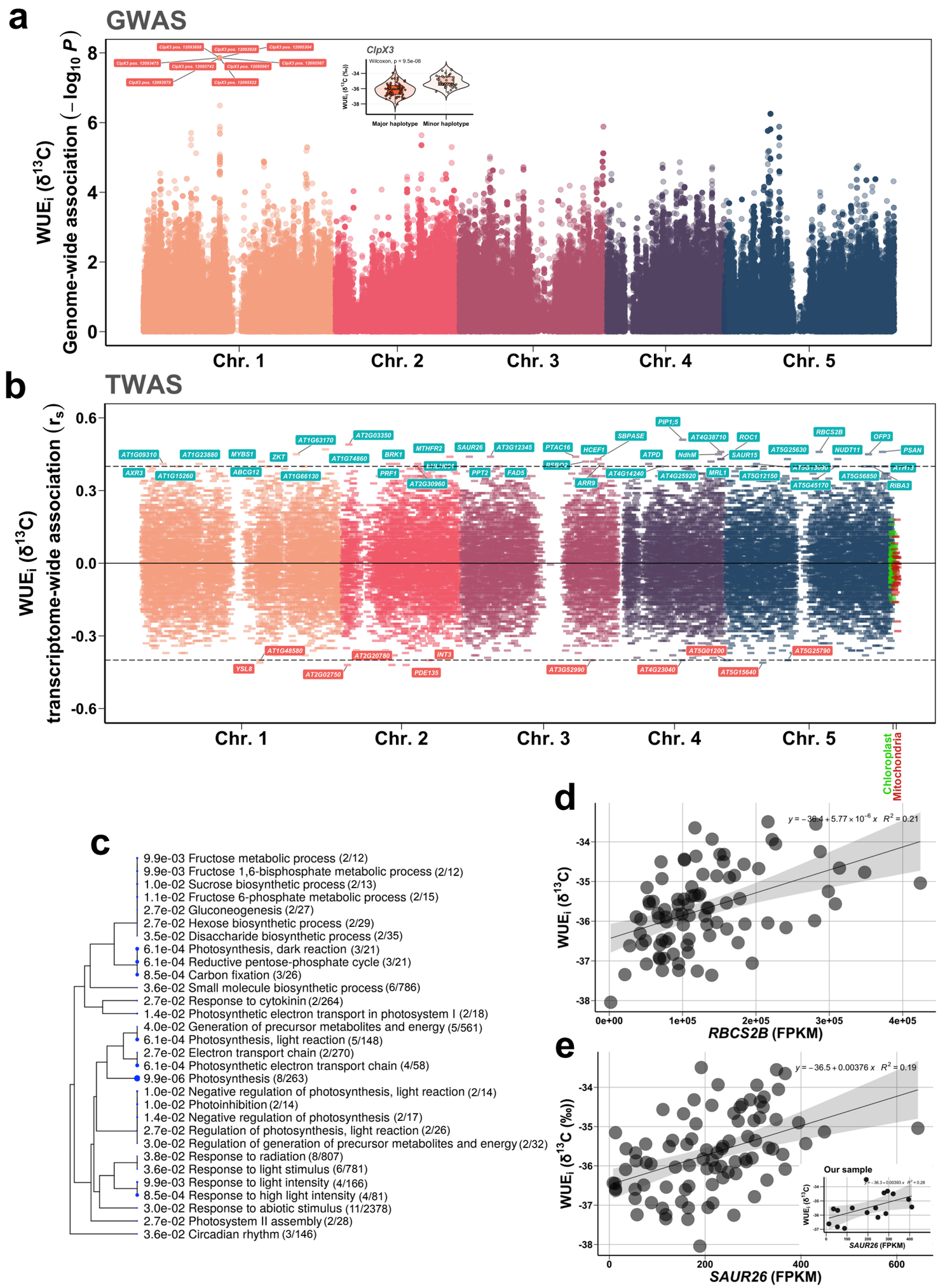

Figure 5. Photosynthesis-related transcript variants regulate water use efficiency in Iberian Arabidopsis accessions. (a) Manhattan plot representing the genome-wide strength of association between genetic variation and variation in δ13C present within 95 Iberian accessions with δ13C values available from (Dittberner *et al.*, 2018). The score (y-axis) consists of the negative logarithm of the *P*-value and provides association strength. **Inset:** Violin plots representing the probability densities of WUE_i for the major and minor allele haplotypes in *ClpX* for the accessions included in 5a. **(b)** T-Manhattan plot representing transcriptome-wide strength of association between variation in transcript abundance (Kawakatsu *et al.*, 2016) and natural variation in δ13C. This analysis was performed on all Iberian accessions with both transcript abundance data (Kawakatsu *et al.*, 2016) and δ13C information (Dittberner *et al.*, 2018) (n = 88 accessions). The relationship is defined by the Spearman's rank correlation coefficient (r_s). Dashed lines define an arbitrary threshold for positive ($r_s \geq 0.4$) or negative ($r_s \leq -0.4$) correlation with water-use efficiency (y-axis). Blue labels highlight the transcripts positively associated with higher WUE_i, while red labels highlight those negatively associated with higher WUE_i. **(c)** Hierarchical clustering tree summarizing the correlation among significant GO Biological Process categories resulting from analysis of the positively correlated candidates resulting from TWA analysis of water use efficiency determined from δ13C values in 88 Iberian Arabidopsis accessions. Ratios provide the number of genes positively correlated with WUE_i within each GO category relative to the total number of genes within that category. The size of the blue dots increases proportionally with P-value significance. **(d)** Scatter plot depicting the positive relationship (*P*-value < 0.05) between WUE_i (y-axis) and *RuBisCO SMALL SUBUNIT 2B* (*AT5G38420*; *RBCS2B*) transcript abundance (x-axis) for the Iberian accessions included in 6b. **(e)** Scatter plot depicting the positive relationship (*P*-value < 0.05) between intrinsic water-use efficiency (WUE_i; y-axis) and ***SMALL AUXIN UP RNA 26*** **(***SAUR26,* **AT3G03850)** transcript abundance (x-axis) for the Iberian accessions included in 6b. **Inset:** Scatter plot depicting the positive relationship (*P*-value < 0.05) between intrinsic water-use efficiency (WUE_i; y-axis) and ***SMALL AUXIN UP RNA 26*** **(***SAUR26,* **AT3G03850)** transcript abundance (x-axis) for the 43 accessions included in our study. For **d)**, and **e)**, gray shadow represents the 95% CI of the fit regression line (black).